Notas de Física - Volume XIV - Nº 7

RADIOCHEMICAL APPLICATIONS OF THE MÖSSBAUER EFFECT*

J. Danon
Centro Brasileiro de Pesquisas Físicas
Rio de Janeiro - Brazil

(Received December 4, 1968)

A basic law of radioactivity is that the chemical conditions of the source do not change the decay constant of the radio-element and do not influcence the energy of the emitted radiations.

This is a consequence of the fact that nuclear processes involve energies of the order of MeV whereas chemical bonding of at most a few eV. However, if we are able to mesure the radio active energy with extreme accuracy we can detect changes of the order of eV in MeV. In such conditions it is possible to observe the influence of chemical bonding on the energy of the nuclear process.

Resonance methods can offer such accuracy. The resonant absorption of a particle occurs only if its energy is precisely that of the nuclear transition (Fig.1). The limit for this precision is determined by the Heisenberg uncertainty principle: the width Γ

* Presented at the II Interamerican Conference on Radiochemistry, Mexico City, May, 1968.

of resonance line times the life time of the nuclear process γ is equal to π (Fig. 2). If E is the energy of the transition the theoretical limit for the accuracy is given by the ratio Γ/E. The value of Γ/E for the 14.4 keV transition of ^{57}Fe to its ground state is 10^{-12}. Thus, changes in the energy of the 14.4 keV gamma ray of about 1 part in 10^{12}, due to the influence of the chemical binding of the iron atom, will perturb the resonance absorption of this photon by the ^{57}Fe nucleus.

The possibility of detecting these extremely narrow nuclear resonance lines was discovered by R. Mössbauer in low energy gamma transition [1, 2].

It has been known for a long time that a basic difficulty for observation of the resonance absorption of nuclear photons comes from the fact that the recoil of the nucleus, due to the emission of the gamma-ray, changes the energy of the emitted radiation. For an isolated nucleus the amount of recoil energy E_R is always much larger than the line width Γ of the nuclear transition, and as a consequence the emitted gamma-ray does not have the correct energy to be absorbed resonantly.

For nuclei which are bound in solids the situation is different. Here the recoil momentum is imparted to the center of mass of the solid. The loss of energy by recoil becomes neglegible since it is whole mass of the solid which is involved in the recoiling process. However, the recoil energy can be dissipated in forms other than kinetic energy, for example by

changing the internal state of the lattice. However, here it is necessary to take into account quantum effects. The permissible internal states of the lattice are quantized elastic waves, or phonons. As a consequence, although the recoil energy of each gamma ray is, on the average, transferred to the lattice, there is a finite probability that any particular event of emission (or absorption) will occur in a recoiless manner. Thus, if no energy is lost in the form of kinetic energy or by changing the internal state of the lattice, all the available energy of the nuclear transition is transfered to the gamma ray. This gamma ray may be resonantly absorbed by a nucleus and it is this recoil less resonant emission and absorption of a gamma rays which is called the Mössbauer effect.

The recoil-free probability, or Mössbauer factor can be calculated with the usual models of the theory of solids and the results lead to the following conclusions:

A - The Mössbauer effect is limited to relatively low-energy gamma transition. Its probability decreases with the exponential square of the gamma ray energy. The effect has been observed up to 155 keV gamma-radiation, which is close to the upper limit of detectability.

B - The larger Mössbauer effects are observed in the more rigid solids, that is, those prossessing large Debye temperatures.

C - The probability of observing the effect increases with decreasing temperature.

The usual method for detecting the Mössbauer spectra are based on the Doppler effect. Due to the narrow line width of the nuclear resonance it is in general enough to give a small Doppler shift, by moving the source or the absorber, to sweep over the resonance. This is the reason why the Mössbauer spectra are usually reported as a function of Doppler velocity. In appendix we list the isotopes in which the M.E. has been observed.

HYPERFINE INTERACTIONS

Due to the narrow linewidth of the Mössbauer nuclear transition, the resonance spectrum is extremely sensitive to energy variations of the gamma radiation. For this reason small interactions between the nucleus and the electrons manifest themselves in the Mössbauer spectra. It is this influence of the electronic environment on the nuclear gamma-transition which determines the hyperfine structure of the Mössbauer spectra. Essentially all Mössbauer spectroscopy is based on these hyperfine interactions.

We shall limit ourselves to some basic definitions and more relevant aspects of these hyperfine interactions, which have been throughly described by several authors [3, 4, 5].

As we shall see in what follows, thse interactions can to a first approximation, be expressed by the product of a term containing only nuclear parameters and another term with parameters of electronic origin. These electronic parameters refer to electric and magnetic effects caused by the orbital electrons in the region of nucleus and they are susceptible to an interpretation in terms of the electronic structure of the atom.

The main interaction which manifest themselves in the Mössbauer effect are:

A. Nuclear isomer shift

B. Nuclear quadrupole coupling

C. Magnetic hyperfine interaction

The nuclear isomer shift manifests itself as a shift of the center of the Mössbauer spectrum from zero velocity (Fig. 3). This is due to the electrostatic interaction between electrons and the nuclear charge distribution:

$$\text{I.S.} = F(Z)\,\frac{\Delta R}{R}\left\{\psi_s^2(0) - \psi_a^2(0)\right\}$$

where F(Z) depends on nuclear parameters, $\Delta R/R$ is the relative variation of the nuclear radius from excited to ground state and the $\psi^2(0)$ are total s-electron densities at the nucleus for the source and absorber.

For the most systems one finds a typical range of values of isomer shift for a given oxidation state. This is one of the bases of the analytical applications of the Mössbauer spectroscopy: identification of oxidation states of an element in a solid through the measured isomer shift.

The nuclear quadrupole coupling is due to the electrostatic interaction between a field gradient at the nucleus with the nuclear quadrupole moment. It splits the Mossbauer spectrum and is a measure the distortion form cubic symmetry around the nu-

cleus (Fig. 4).

For some systems we also find typical ranges of quadrupole splitting for different oxidation states of an element. Thus besides the main application, which gives direct information on the symmetry of a molecular environment, it is also possible in many cases to identify an oxidation state from the quadrupole coupling value. Intensities, angular variation and temperature of the quadrupole lines can also yield valuable information on chemical binding.

The magnetic hyperfine splitting is due to the interaction of the nuclear magnetic moment with a magnetic field. It also splits the spectrum in a characteristic way (Fig. 5). The magnetic field acting at the nucleus is usually called the internal field.

The magnetic hyperfine structure of the Mössbauer spectra depends of the magnetic state of the sample: paramagnetic, ferromagnetic and anti-ferromagnetic. For the paramagnetic ones it is important to take into account the electronic relaxation. If it is slow compared with nuclear lifetime it will produce a field seen by the nucleus (Fig. 6). Otherwise no field will split the Mössbauer spectrum.

Internal fields have also values which are dependent on oxidation states of an element, and on the state of chemical binding.

We will now review the present state of the most important applications of the Mössbauer effect to radiochemistry.

1. RADIOLYSIS OF SOLIDS

The information of different oxidation states and changes in symmetry of surroundings of an atom, induced by radiation, can be detected "in situ" without any perturbation of the conditions under which it was formed.

A first example was given by Saito and collaborators [6] who showed that the Mossbauer spectrum of pure ferric oxalate exibits new lines when irradiated with gamma-rays, typical of iron $^{+2}$ salts (Fig. 7).

More recently Wignall [7] observed the formation of divalent tin due to radiation damage from thermal neutron capture of magnesium tin oxide Mg_2SnO_4 (Fig. 8).

Investigating the decomposition of sodium nitroprusside by 2 MeV electrons by the Mossbauer effect we have found the formation of a ferric-ferrous cyanide complex similar to Turnbull's blue, which gives a typical spectrum of high-spin iron+3 and low-spin iron + 2 (Fig. 9).

RECOIL CHEMISTRY

The Mössbauer source is an isotope which by radioactive decay populates the Mössbauer transition, such as the K-capture in ^{57}Co giving ^{57}Fe, or is induced by a nuclear reaction such as

(n, γ), Coulomb excitation, etc. (Fig.10).

In any case we have a nuclear process preceding the Mössbauer transition, which can change the chemical state of the original atom. Thus, the electron capture is generally followed by Auger electron emission: following K-capture, while one electron from an outer shell drops into the inner hole a second one is elected from the atom to carry off the excess energy. This can lead to the formation of highly ionized atomic states. In gases this has been beautifully demonstrated using a magnetic deflection spectrometer to separate the charge states produced after internal conversion in ^{131}Xe. It was found that the most probable charge state is Xe^{+8}.

In solids we know that these highly charged states will rapidly disappear, since electrons can be captured from the neighboring atoms.

The Mössbauer effect can give two types of information for this phenomena:

A - through characteristic isomer shifts, quadrupole splittings and internal fields identify a given charge state.

B - Give limits for the lifetime of a given state.

Let us assume that in a source, carefully prepared, containing only Co^{+2}, one finds besides the ferrous line the ferric one.

If we assume that the ferric state decays exponentially to

the ferrous state it is possible to see a linewidth for the trivalent iron large than the nuclear lifetime. From these line broadening effects it is possible to estimate the lifetime of the Auger formed oxidation state. The limits of applicability of this method is given by:

$$0.1\tau < \theta < 10\,\tau$$

where τ is the nuclear lifetime.

A system which has been several times investigated is cobaltous oxide, CoO. Starting with ^{57}CoO and using a single line absorber, one gets two lines, one for Fe^{+2} and the other for Fe^{+3}. This is confirmed by typical hyperfine splitting below the Neel temperature (Fig. 11).

Since Fe^{+3} has a broader line, one can estimate the lifetime for this state in the Cobaltous oxide. However, there is no agreement between the results of several investigators. A decisive experiment was made [12] by using delayed coincidences for measuring the real lifetime of the trivalent state. It was concluded that the trivalent iron formed is stable, or in other words, that the charge states observed are established in a time short compared with the nuclear lifetime of 10^{-8} sec.

The explanation for the formation of a relatively large Fe^{+3} fraction and its broadening can be found by assuming that this formation is due to the stabilization of Fe^{+3} in the vicinity of a metal ion vacancy in the oxide. However, it is necessary to take into account not only an iron atom next to a vacancy but

also at some distance from it. The existence of a range of interaction between the iron and the vacancy can explain the broadening reported for the line of Fe^{+3}, which was erronously attributed to the decay of this state.

A number of other systems have been investigated in search for Auger after-effect produced change states and for possible life time effects: ^{57}Co in $CoCl_2$, ZnF_2, NaF, $BaTiO_3$, CoSi.

After effects have also been investigated in cobalt acetyl acetonate and cobalticinium tetraphenylborate [13]. The formation observed of Co^{+3} from a trivalent cobalt salt cannot be explained from Auger effect change state theory. A possible reason is that the Auger process disrupts the molecule and provides electrons which are trapped in the iron atoms whose environment then rearranges to accomodate the new valence state.

Similar experiments have been made with hydrated salts [14, 15] such as Co $SO_4 \cdot 7H_2O$, Co $Cl_2 \cdot 6H_2$, Co $SO_4(NH_4)_2 \cdot 6H_2O$, Co Si $F_6 \cdot 6H_2O$ and $Fe(NH_4)_2$ $SO_4 \cdot 6H_2O$. The presence of water molecules is a great importance in stabilizing states such as Fe^{+3} and perhaps Fe^{+4} (Fig. 12).

As a consequence of the isomeric decay of $^{119}Sn^{m}O_2$ new lines are apparent in the Mössbauer spectra [16] and were attributed to after effects.

When one uses ^{241}Am in insulators for populating the 55 kev Mössbauer line of ^{237}Np and measures it against a single line absorbed such as NpO_2, a multiline Mössbauer spectra is obtained [17].

The lines are due to different charge states of ^{237}Np recoil atoms following alpha decay of ^{241}Am (Fig. 13).

An example of Mössbauer effect obtained by nuclear reaction[18] is the population of the 29.4 kev transition in ^{40}K from the reaction $^{39}K(n,\gamma)^{40}K$. The emission of energetic gamma rays preceding the formation of the 29.4 kev state leaves the ^{40}K with a distribution of recoil energies up to 800 kev. Such energies should displace the potassium atoms out of their normal positions in the lattice. It is however impressive that both the factor and the line width are not makedly affected as was observed in the Mossbauer spectra of KF and KCl.

SURFACE STUDIES WITH THE MÖSSBAUER EFFECT

A number of important radiochemical methods involve heterogeneous equilibria with a presence of a solid phase.

Surface phenomena, such a absorption, nucleation and others are of basic importance in these equilibria.

The possibilities of using the Mössbauer effect in surface studies seem very promising.[19] The Mössbauer parameters are sensitive to the anisotropy which prevails at an atom on its surface. Thus, the recoil-free fraction depends on the mean-square displacement of the emiting nucleus from its equilibrium position. This displacement is expected to be different on the surface than in the bulk of the cristal and it should also depend on the direction of the gamma ray (Fig. 14).

The anisotropy should also induce local field gradient and consequent quadrupole splitting on the spectra. The angular variation of the quadrupole splitted lines should also reflect this situation.

Although the conditions appear to show great potentialities only a limited number of investigations have been conducted. This is mainly due to experimental difficulties in asserting that the atom is really at the surface, in avoiding contamination of the surface, etc.

The first system investigated [20] was ^{57}Fe in Al_2O_3. A more detailed study has been made with ^{57}Co on policrystaline tungsten [21]. For temperatures between 100 - 500°K and angles between 0° and 60° the spectrum obtained is a broad line, which has been fitted by 3 different lines. The Mössbauer parameters of two of the lines are attributed to surface quadrupole splitting. (Fig. 13).

MÖSSBAUER EFFECT IN MICROCRYSTALS

The Mössbauer effect has been detected in disperse systems and this can be of interest for the study of radiocolloids.

The effect was observed in ^{197}Au microcrystals which were grown in a hydrosol and bound in gelatin [22]. The results with 60 and 200°A, at 4.2 and 63°K, indicate that the crystal surfaces are loosely bound to gelatin and that the recoil-free fraction is greater in the smaller microcrystals than in the

larger ones. The size dependence is a consequence of the contribution of the surface of the microcrystals to the recoil-free fraction (Fig. 16).

The Mössbauer effect has also been detected in a dispersed system: $^{119}Sn^{m}O_2$ in glycerine or castor oil. [23] Particles with 2.5×10^{-5} cm of radius give a spectra with a brodened width. This broadening exibits the expected dependence of the Brownian motion of the particles.

MÖSSBAUER EFFECT IN ION-EXCHANGE RESINS

Information on the nature of the species adsorbed in ion-exchange resins and the type of binding is of importance and not easily obtained with the usual spectroscopic methods.

The Mössbauer effect can be detected in dried resins and wet resins which are frozen to liquid nitrogen temperatures. No effect is detected in resins in equilibrium with water at room temperature [24] (Fig. 17).

Typical high-spin ferrous and ferric salts and low-spin iron complexes such as $Fe(CN)_6^{4-}$ and $Fe(CN)_6^{3-}$ were investigated after equilibration with both cation and anion-exchange resins.

The comparison of isomer shifts and quadrupole splittings for the absorbed species with that of the pure salts shows that Fe^{+2} and the complex cyanide ions are not affected by the picture in which the ions in the resin retain their primary hydration shells and interact electrostatically but non-specifically with

with the resin ionogenic groups.

With Fe^{+3} ions two types of species were observed which depend on the resin moisture content. This can be explained by the hydrolysis of the Fe^{+3} ions in the resin with formation of an iron dimer and ferric oxy-hydroxide (Fig. 18).

MÖSSBAUER EFFECT IN SOLUTIONS

Although the Mössbauer effect is a typical solid state phenomena, it has been observed in liquids [25, 26]. The conditions for this observation are quite restrictive since they require high viscosity of the liquid and low temperature of the system. Moreover, the spectra obtained are always broadened as a consequence of the diffusive motion of the ions in the liquid.

The first systems investigated were ferrous and ferric sulfate in glycerol [25]. The spectra obtained were typical of these oxidation states of iron, that with the Fe^{+2} presently the quadrupole splitted lines (Fig. 19). Until now these results have been used only in diffusion studies. In a recent work [27] using both absorption and scattering measurements with Fe^{+2} and Fe^{+3} in glycerol it has been shown that "jump" diffusion mechanism of the Fe^{+3} ion is larger than the "continuous" type of diffusion.

A technique which has been used in order to apply the Mössbauer effect to solutions is to freeze the solution, which becames a solid and the effect is normally detected.

The first investigations were made with aqueous solutions of

Fe^{+2} and Fe^{+3} salts, the spectra being recorded after dipping the solution rapidly into liquid nitrogen [28]. The comparison of the spectra obtained with that of the pure salts shows that the Mössbauer patterns of the frozen solutions exhibit a different temperature dependence of the intensity of the effect and a larger value of the linewidth. The quadrupole splitting and isomer shifts are however close to the values obtained with the pure salts.

A detailed investigation with frozen aqueous solutions of ferrous chloride and sulfate has been made recently [29]. In these conditions the ions are trapped in ice and the Mössbauer effect allows a detailed study of the symmetry of the ice molecules around the ferrous ion, together with interesting phase changes in the ice-salts system (Figs. 20, 21, 22).

Although these results are of interest in themselves, from a radiochemical point of view the more important fact is that the values of the hyperfine interaction in the frozen solutions do not differ markedly from that obtained in the pure salts. It is thus possible to use the Mossbauer spectra to help to identify chemical species in solution.

A very interesting result has been recently obtained [30] regarding the Mössbauer effect in frozen solution. The isomeric shifts of Sn(IV) in frozen solution has been measured as a function of concentration of added H X X = F, Cl, Br and I).

Fig. 23 illustrates the results obtained. It is seen that the isomer shift changes with the X^- concentration and tends at

the limit to the value observed in the corresponding tin (IV) complex halide.

The isomer shift of Sn(IV) appears to be a linear function of the number of its attached halide ions. The results support the observation that for the Sn(IV) halide complexes the stability increases in the order Br^-, Cl^-, F^- since the saturation value of the isomer shift occurs in relatively lower concentrations F^+, Cl^- and Br^-.

This technique offers a new method for investigating equilibria among complex ion in solution.

These possibilities in solvent-extraction processes have been recently demonstrated [31] (Fig. 24). Conventional solvent-extraction studies have established that the chloro and bromo complexes extracted by nitrobenzene from iron (III) in chloride and bromide solutions are the anions $Fe\ X_4^{-1}$. The Mössbauer spectra of the frozen extract from 0.02 M in iron (^{57}Fe enriched) and 8M - HBr gives an isomer shift of 0.45 mm/sec. with respect to stainless steel and no quadrupole coupling. This is in agreement with the presence of a 4 - coordinate high spin Fe^{+3} complex with the ligand equivalent. Similar results were obtained with frozen extracts of chloride solutions.

With thyocianate systems, in conditions where enough iron goes to the organic phase, a mole ratio Na: Fe: SCN = 1 : 1 : 4. is found in the extract. It might appear that the iron complex involved is simply $Fe(SCN)_4^{-1}$. However the Mössbauer spectrum

shows a quadrupole splitting of 0.56 mm/sec. and isomer shift of 0.61 mm/sec. with respect to stainless-steel. The presence of a quadrupole splitting indicates a low symmetry surroundings for the high-spin Fe^{+3} complex. It is possible that the species undergoing extraction is $Fe(SCN)_4X_2^{-1}$ where X stands for water or nitrobenzene.

In some systems the Mössbauer spectra of the solvent extracts shows the typical effect of slow relaxation phenomena.

CHEMISTRY AND SOLID STATE PROPERTIES OF THE HEAVIEST ELEMENTS

Nearly every element with atomic number larger than 90 is a potential candidate for Mössbauer effect experiments by the fact that they have a low-energy gamma transition to the ground state. Thus, Mösshauer spectroscopy offers a new technique for chemical and solid state investigations in this region of the periodic chart. Even though other types of limitations to the detectability of the Mössbauer effect in such elements were take into account, 25 possible candidates were still listed in a first study in this field. [32]. At the present moment the Mössbauer effect has been detected in ^{237}Np, ^{238}U and ^{231}Pa. The 59.6 keV transition in ^{237}Np was the first in which the effect has been observed and at present an impressive number of applications have been demonstracted [33].

(A) Correlation of the isomer shift with oxidation state.

It has been found that each oxidation state of Np compounds has a characteristic range of isomer shift and other than for Np(0) these ranges are widely separated (Fig. 25).

Besides the practical interest for the identification of the oxidation state of neptunium in a given compound, this result has been analyzed in terms of the electronic structure of neptunium. It is suggested that there are no 7s electrons and there are only 5f electrons in the valence shell. The closed-shell 6s electrons are shielded from the nucleus by the 5f electrons; therefore, the density of 6s electrons at the nucleus decreases a more 5f electrons are added (decreasing oxidation number). Thus, isomer shifts would increase with decreasing oxidation number. This interpretation is consistent with the fact that Np(0) compounds do not follow the trend, since their valence shell presumably contains 7s and 6d as well as 5f electrons.

(B) Correlation with quadrupole coupling

An interesting correlation exists between the quadrupole couplings and the isomer shift of the neptunium compounds. This correlation shows that distinct ranges of values of quadrupole couplings are obtained with the different oxidation states of the element (Fig. 26). The potential uses of this result for chemical applications are evident.

However, an explanation for this result is still required. For the oxigenated $Np{=}O^{+}$ and NpO^{2+}, large electric field gradients are

expected since these species are linear O-Np-O. Indeed the experimental results show much larger quadrupole couplings for oxygenated Np(V) and Np(VI) compounds than for non-oxygenated Np(III) and Np(IV) compounds.

A number of possible investigations in the chemical bonding in neptunium compounds using these results have been discussed[32].

(C) Charge states after alpha decay

As mentioned previously, sources of ^{241}Am in insulators give multiline spectra which are due to several oxidation states of ^{237}Np formed after alpha-decay of ^{241}Am. This offers new possibilities for the study of recoil-chemistry for the heaviest elements.

A number of other physical studies of the actinide elements, such as magnetic investigations, nuclear polarization effects, etc. are possible on the basis of the Mössbauer spectroscopy.

APPENDIX

ISOTOPES IN WHICH THE MÖSSBAUER EFFECT HAS BEEN OBSERVED

Mössbauer Isotope	Abundance of Stable element %	Gamma-ray energy (kev)	Half-life of Mössbauer transition (10^{-9}s)	Parent Isotope	Half-life of Parent Isotope
^{40}K	0.0118	29.4	3.9	^{39}K	(n, γ) reaction
^{57}Fe	2.19	14.4	98	^{57}Co	270d
^{61}Ni	1.19	67.4	5.3	^{61}Cu	33h
^{67}Zn	4.11	93	9400	^{67}Ga	78h
^{73}Ge	7.80	67.0	2.33	^{73}Ge	Coulomb Excit
^{83}Kr	11.55	9.3	147	^{83}Rb	83d
^{99}Ru	12.72	90	20	^{99}Rh ^{99}Tc	16d 2.1×10^{5}y
^{119}Sn	8.58	23.8	18.5	^{119m}Sn	245d
^{121}Sb	57.25	37.2	3.5	^{121m}Te	154d
^{125}Te	6.99	35.6	1.4	^{125}I	57d
^{127}I	100	59	1.8	^{127}Te ^{127}Xe	105d 36d
^{129}I	adioac	26.8	16.3	^{129m}Te	33d
^{129}Xe	26.44	40	0.96	^{129}I	1.6×10^{7}y

Mössbauer Isotope	Abundance of Stable element %	Gamma-ray energy (kev)	Half-life of Mössbauer transition (10^{-9}s)	Parent Isotope	Half-life of Parent Isotope
^{131}Xe	12.18	80.2	0.50	^{131}I	8.1d
^{133}Cs	100	81	6.23	^{133}Ba	7.2y
^{141}Pr	100	145.0	2.0	^{141}Ce	33d
^{149}Sm	13.83	22	7.6	^{149}Eu	106d
^{151}Eu	47.82	21.6	8.8	^{151}Gd ^{151}Sm	120d 93y
^{152}Sm	26.63	122	1.4	^{152}Eu	9h
^{153}Eu	52.18	97.5 103.2	0.14 3.8	^{153}Gd	242d
^{155}Gd	14.73	86.5	5.86	^{155}Tb ^{155}Eu	5d 1.81y
^{156}Gd	20.47	89	1.9	^{155}Gd	(n,γ) reaction
^{158}Gd	15.68	79.5	-	^{157}Gd	(n,γ) reaction
^{159}Tb	100	58	0.13	^{159}Dy	144d
^{160}Dy	2.29	86.8	2.05	^{160}Tb	72.4d
^{161}Dy	18.88	25.6 74.5	28 3.0	^{161}Tb	6.9d
^{166}Er	33.41	80.6	1.83	^{166m}Ho	>30y
^{169}Tm	100	8.41	3.9	^{169}Er ^{169}Y	9.4d 32d
^{170}Yb	3.03	84.2	1.61	^{170}Tm	127d
^{171}Yb	14.31	66.7	0.5	^{171}Tm	1.9y

Mössbauer Isotope	Abundance of Stable element %	Gamma-ray energy (keV)	Half-life of Möss - bauer tran sition (10^{-9} s)	Parent Isotope	Half-life of Parent Isotope
^{177}Hf	18.50	113	0.52	^{177}Tu	68d
^{181}Ta	39.99	6.25	6800	^{181}Hf ^{181}W	45d 140d
^{182}W	26.41	100.1	1.4	^{182}Ta	115d
^{183}W	14.40	46.5 99.1	0.15 0.52	^{183}Ta	5d
^{186}Os	1.64	137.2	0.84	^{186}Re	90h
^{187}Re	62.93	134.2	0.01	^{187}W	24h
^{188}Os	13.3	155.0	7.2	^{188}Ir	41h
^{191}Ir	37.3	129.4	0.13	^{191}Os ^{191}Pt	15d 3d
^{193}Ir	62.7	73	6.0	^{193}Pt ^{193}Os	500y 32h
^{195}Pt	33.8	98.9 129.7	0.17 0.55	^{195}Au ^{195}Ir	192d 2.3h
^{197}Au	100	77.3	1.8	^{197}Hg	65h
^{237}Np	radioac	59.6	63	^{237}U ^{241}Am	6.75d 458y
^{231}Pa	radioac	84.2	41	^{231}Th	25.6h
^{238}U	radioac	44.0	0.02	^{238}U	Coulomb Excit
^{232}Th	radioac	49.8	0.33	^{232}Th	Coulomb Excit

FIGURE CAPTIONS

Fig. 1: Schematic illustration of resonance scattering of photons: decay of the excited level of the source S with emission of a photon $h\nu$ which is absorbed and reradiated by the absorbed A.

Fig. 2: Excitation probability W(E) versus energy of resonance radiation.

Fig. 3: Isomer shifts of various ^{57}Co sources for a $K_4|Fe(CN)_6|3H_2O$ absorber: (a) ^{57}Co in Pt, (b) ^{57}Co in Pd and (c) ^{57}Co in Vacromium. From W. Kerler et al. Z. Physik 173, 321 (1963).

Fig. 4: Quadrupole splitting of ^{57}Fe in $Na_2|Fe(CN)_5|2H_2O$.

Fig. 5: Magnetic hyperfine splitting of ^{57}Fe in α- Fe_2O_3. From G.G. Kleiner and A. W. Sunyar, Phys. Rev. Letters 3, 412 (1960).

Fig. 6: Magnetic hyperfine splitting due to slow relaxation in glassy and crystalline ferric m-phosphate. From C. R. Kurkian and D. N. E. Buchanan, Phys. Chem. Glasses 5, 63 (1964).

Fig. 7: Mössbauer resonance absorption spectra at 22°C.
(a) Non-irradiated ferric oxalate
(b) Irradiated ferric oxalate
(c) Non-irradiated ferrous oxalate
From N. Saito et al. in "Applications of the Mössbauer Effect In Chemistry and Solid State Physics", International Atomic Energy, Technical Report N° 50, Vienna 1966.

Fig. 8: Effect of (n, gamma) radiation damage on the ^{119}Sn Mössbauer spectrum in $Mg_2\,^{119}SnO_4$ (Versus an SnO_2 absorber). Positive velocity denotes approach of absorber to source. From P. Hannaford, C. J. Howard and J. W. G. Wignall, Phys. Letters 19, 257 (1965).

Fig. 9: Velocity spectrum of a ferri-ferrocyanide complex formed by irradiation of sodium nitroprusside by electrons. The $Fe^{II}(CN)_6$ is responsible for the largest single peak and the two smaller lines on the right are the result of quadrupole splitting of high-spin Fe(III). From J.Danon, R. P. A. Muniz, L. Tosi and A. O. Caride, unpublished results.

Fig. 10: Coulomb excitation of the 137 keV level of ^{57}Fe, which by decay populates the 14.4 Mossbauer level.

Fig. 11: The hyperfine splitting spectra of Fe^{+2} and Fe^{+3} produced by decay of ^{57}Co in CoO:
(a) above the Neel temperature of 291°K and (b) below the Neel temperature. From H. H. Wickman and G. K. Wertheim in "Chemical Applications of Mossbauer Spectroscopy", page 610, Academic Press New York (1968).

Fig. 12: Velocity spectra at several temperatures and atmospheric pressure for $^{57}Co(^{57}Fe)$ in powdered $CoSO_4 \cdot 7H_2O$ which transforms to $CoSO_4$ at high temperatures. Positive velocity corresponds to the absorber approaching the source. From R. Ingalls and G. De Pasquali, Phys. Letters 15, 262 (1965).

Fig. 13: Velocity spectra of several ^{241}Am sources (insulators) showing charge states after alpha decay (Np O_2 absorber). From W. L. Pillinger and J. A. Stone, "Methodology of the ^{237}Np Mossbauer Effect" U.S.A.E.C. AT (07-2-1),1968.

Fig. 14: Typical positions of a nucleus under going a Mossbauer transition. Nucleus B sitting in the surface will show a smaller recoil-free fraction f along the normal $\bar{n}$ than perpendicular to it, whereas nucleus C sitting on the surface should display its largest f along the normal. From J. W. Burton, H. Frauenfelder and R. P. Godwin, in "Applications of the Mossbauer Effect to Chemistry and Solid State Physics", International Atomic Energy Agency, Vienna (1966).

Fig. 15: Mossbauer spectra on polycrystalline tungsten at 100°K From J. W. Burton, Thesis, University of Illinois, February 1965.

Fig. 16: Recoil-free fractions versus absorber temperature for gold microcrystals. Source temperature is 42°K. The dashed curve is calculated for bulk gold using Θ_M = 0°K and Θ_D = 163°K.

Fig. 17: Mossbauer spectra of vaccuum chied Fe^{+3} - 8% cation resin at - 195°C From ref. 24.

Fig. 18: Mossbauer spectra of wet Fe^{+3} - 8% cation resin at - 195°C. From ref. 24.

Fig. 19: Resonance absorption for a solution of enriched iron sulphate in glycerol. (a) - 100°C and - 5°C, dotted line ferrous doublet. (b) 0°C, dotted line Fe^{+3}, dashed lines Fe^{+2}. From ref. 27.

Fig. 20: Isomer shifts and linewidths observed in the ferrous chloride studies. From ref. 29.

Fig. 21: Temperature dependence of the Mossbauer quadrupole splitting for 0.47M frozen ferrous chloride solutions which were quenched from the liquid state to - 196 °C and then warmed up slowly. In the transition region indicated by the dashed line, the Mossbauer effect disappears for a period of time and then reappears with the larger quadrupole splitting. From ref. 29.

Fig. 22: Isomer shifts and line widths observed in the ferrous sulphate studies. From ref. 29.

Fig. 23: Curves showing the variation of the isomer shift as a function of the concentrations of the indicated solvents. The labels |H Br|, |HCl| and |HF| indicate that the isomer shift was measured with 0.22 molar

$Sn\ Cl_4$ mixed with increasing concentration of these solutions. The curve labeled $|Sn\ Cl_4|$ was obtained by varying the concentration of $Sn\ Cl_4$ in pure water. From ref. 30.

Fig. 24: Spectra of nitrobenzene extrats of ^{57}Fe - enriched iron from HBr(A) and NaSCN(B) solutions. From ref. 31.

Fig. 25: ^{237}Np isomer shift ranges for the different neptunium oxidation states (relative to $Np\ O_2$) From ref. 33.

Fig. 26: Correlation between quadrupole coupling contants (1/4 eqQ) and isomer shift (relative to $Np\ O_2$) for neptunium compounds representative of ^{237}Np oxidation states. From ref. 33.

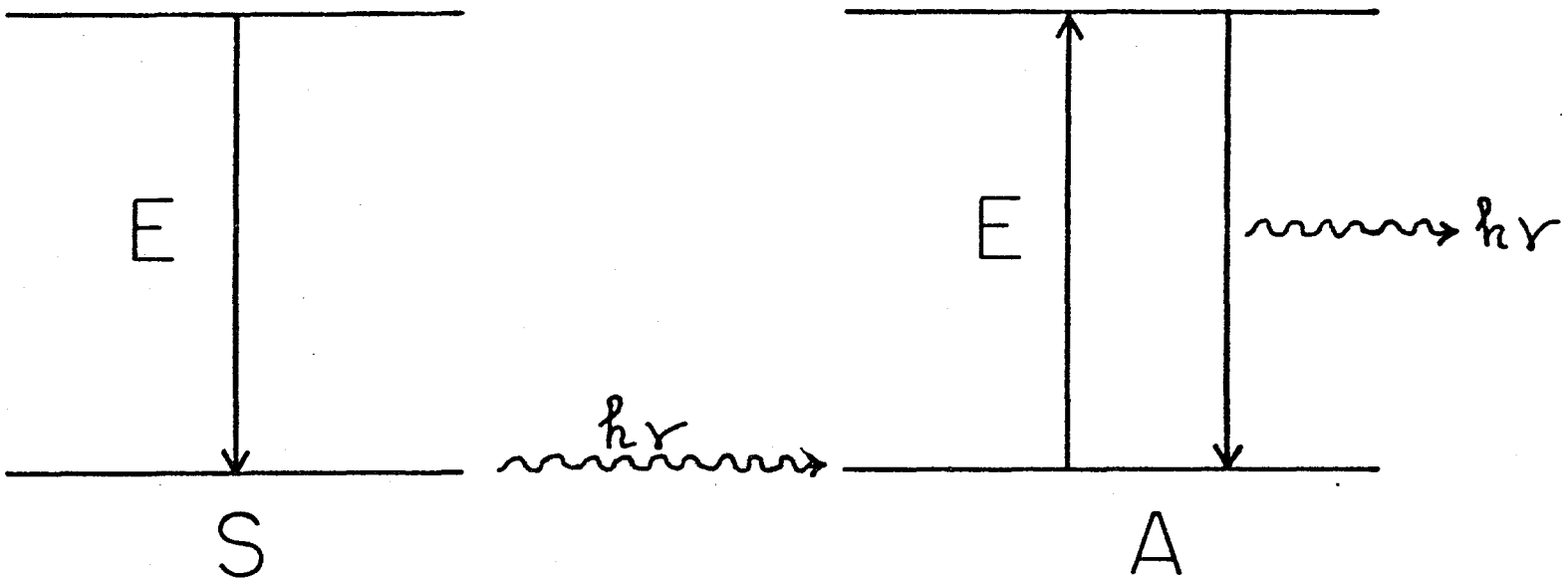

FIG. 1

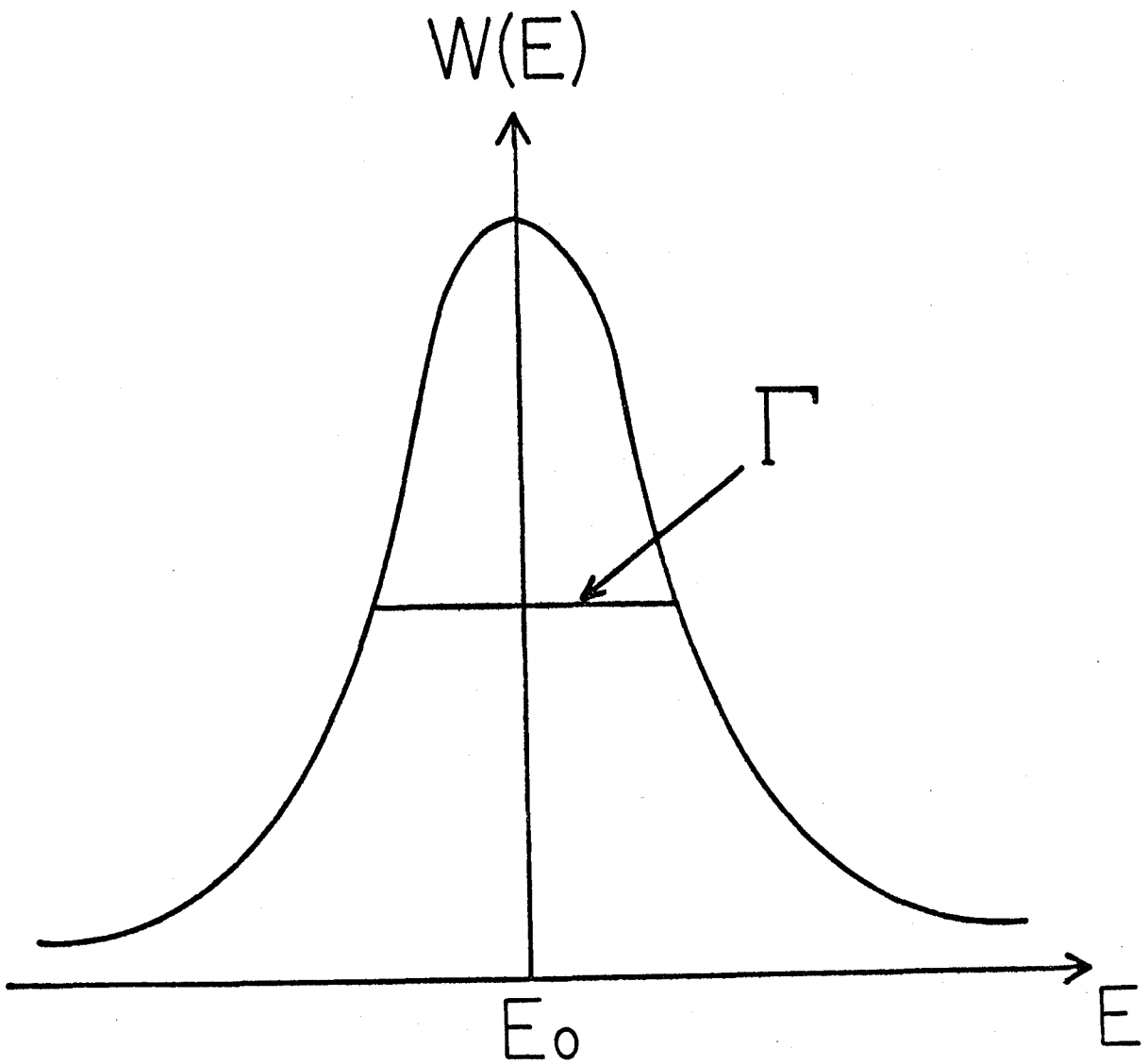

FIG. 2

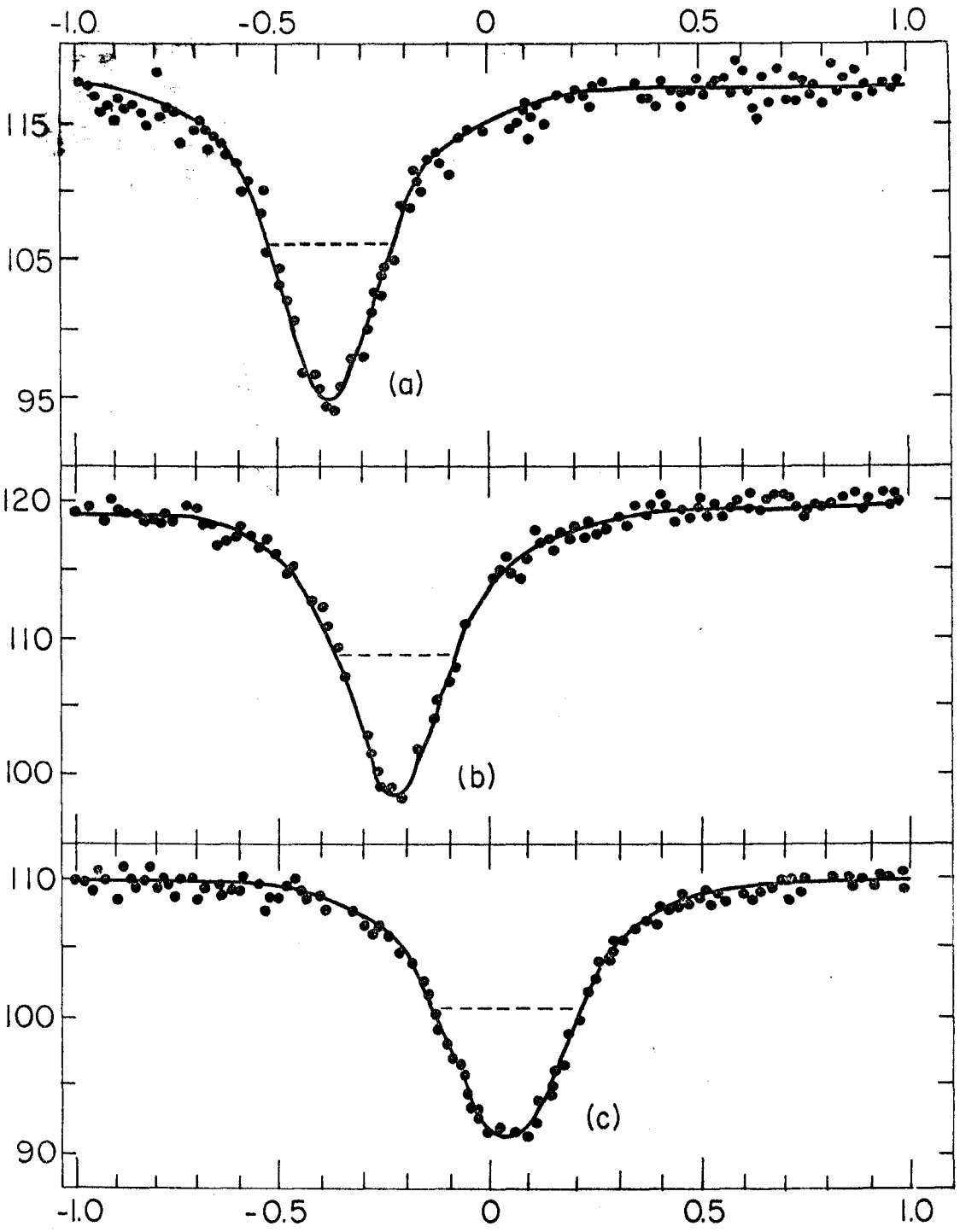

FIG. 3

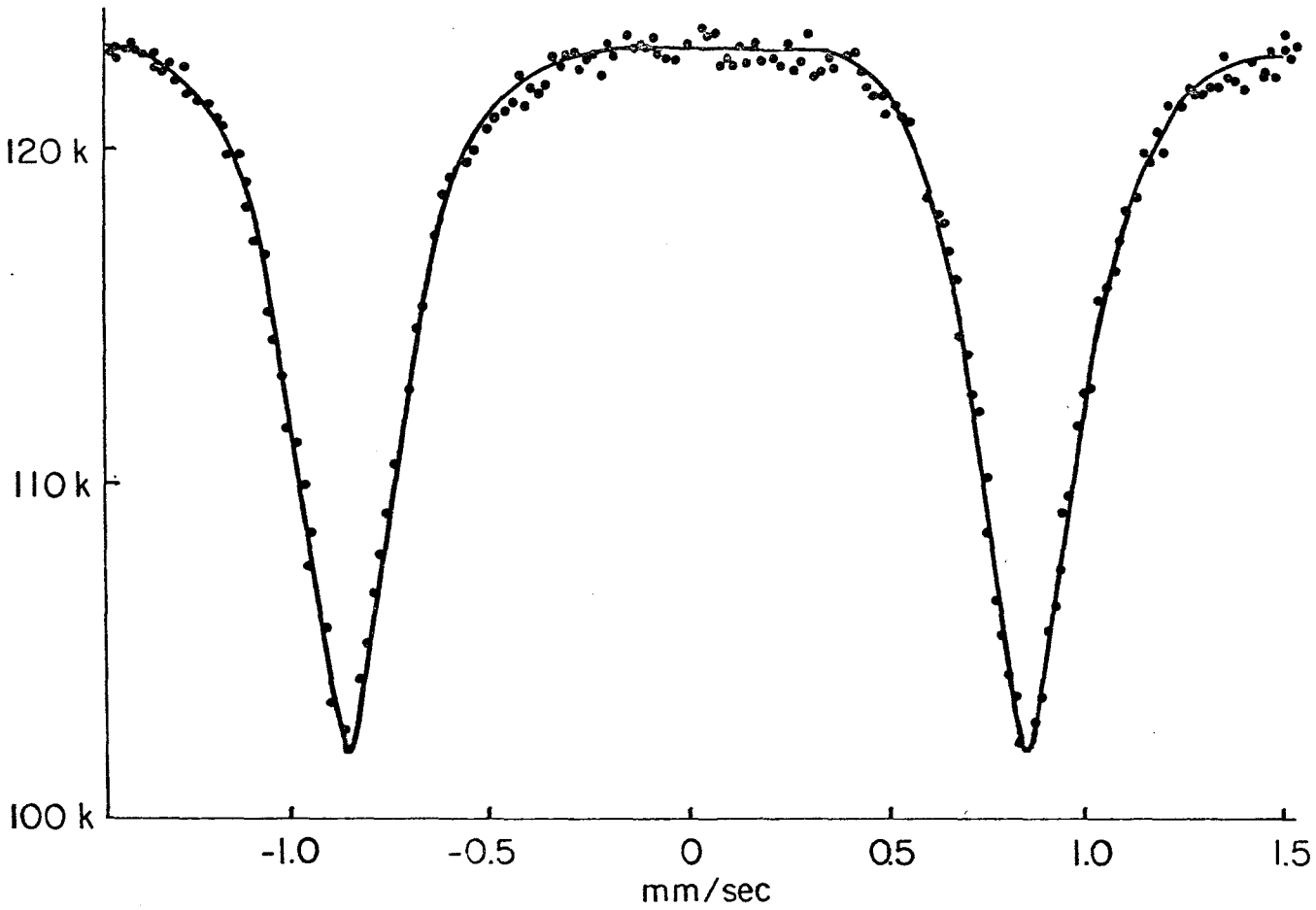

FIG. 4

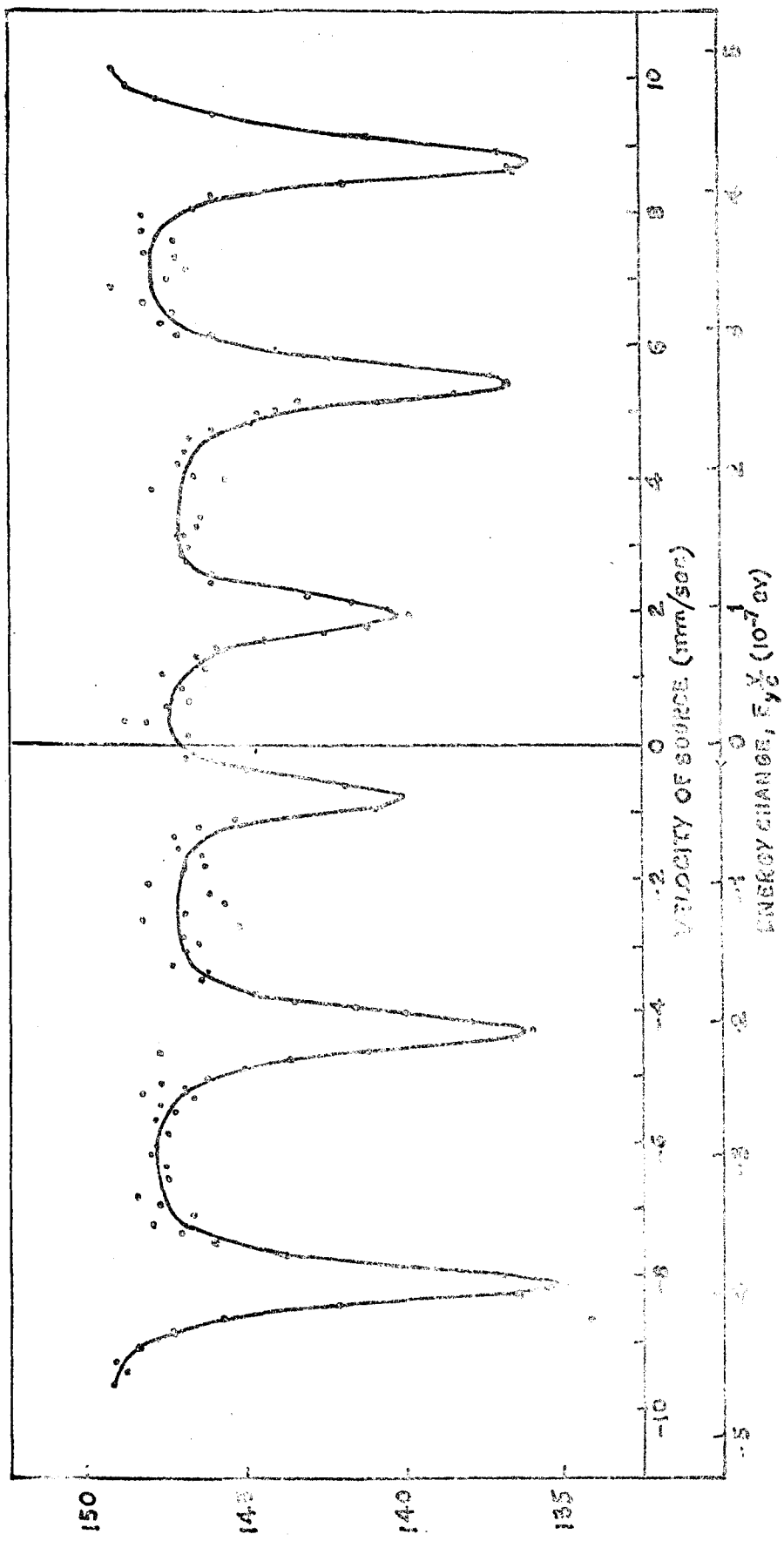
150
145
140
135
-10
-8
-6
-4
-2
0
2
4
6
8
10
VELOCITY OF SOURCE (mm/sec)
ENERGY CHANGE, E γ2 (10⁻⁴ ev)

FIG. 5

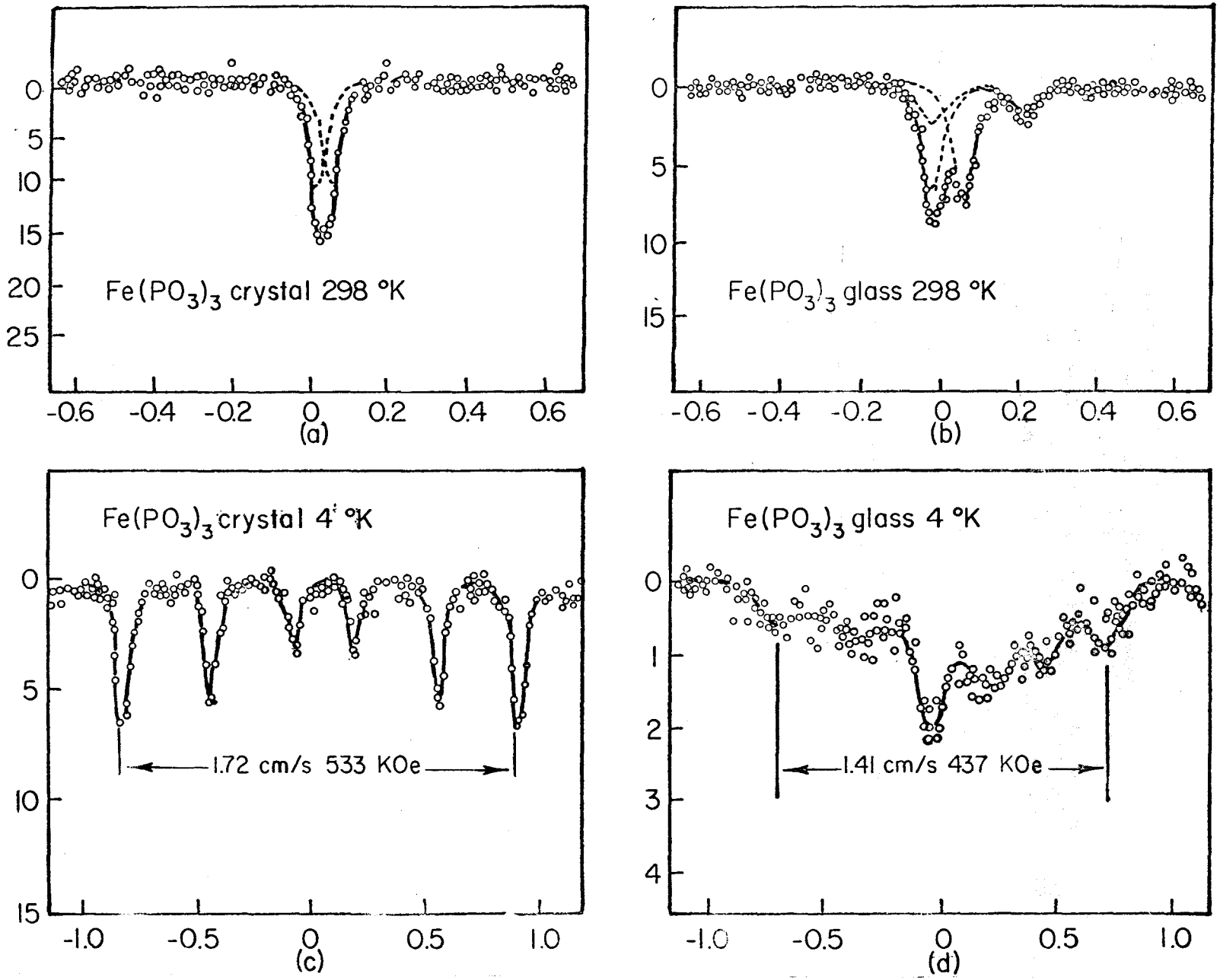
Fe(PO3)3 crystal 298 °K
(a)
Fe(PO3)3 glass 298 °K
(b)
Fe(PO3)3 crystal 4 °K
1.72 cm/s 533 KOe
(c)
Fe(PO3)3 glass 4 °K
1.41 cm/s 437 KOe
(d)

FIG. 6

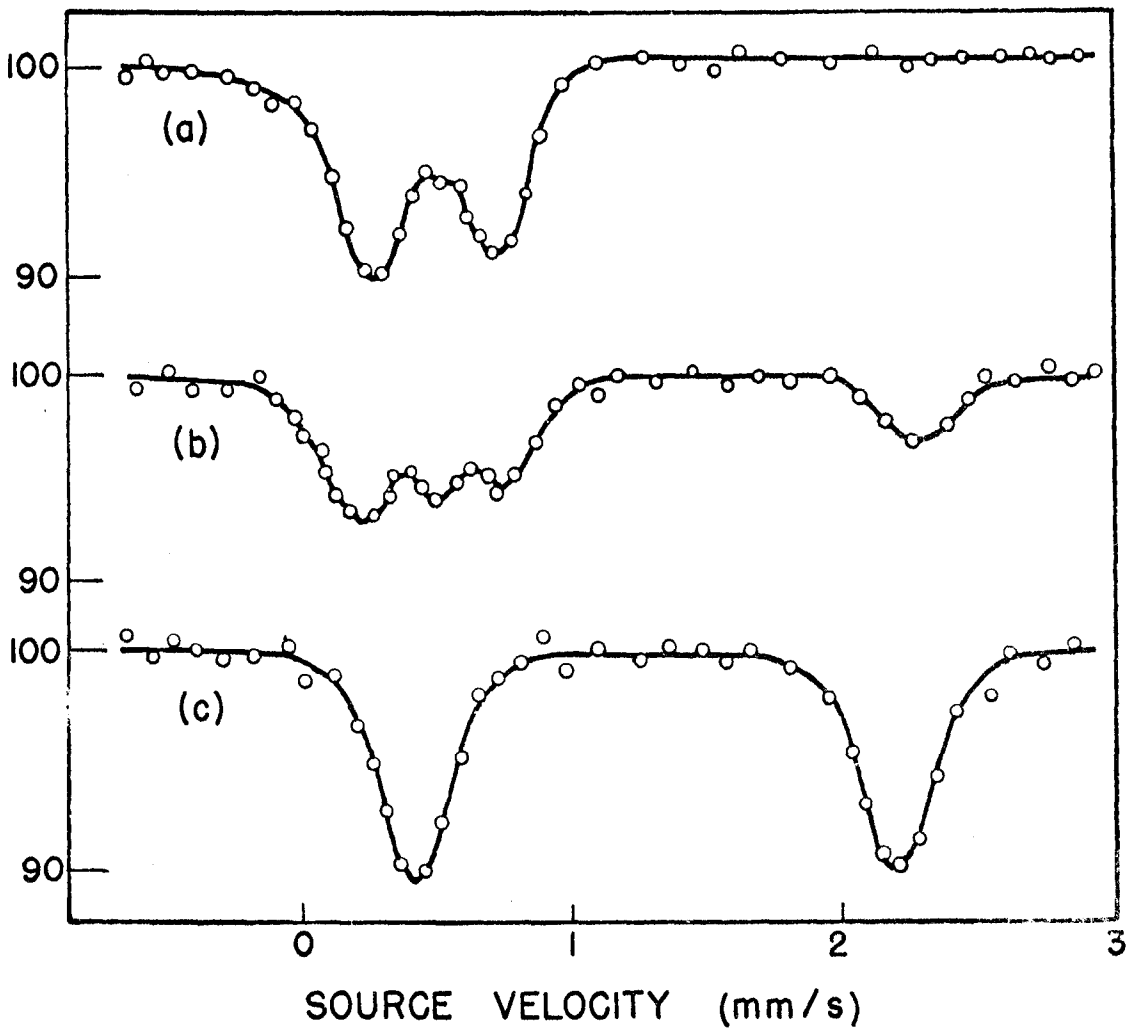

FIG. 7

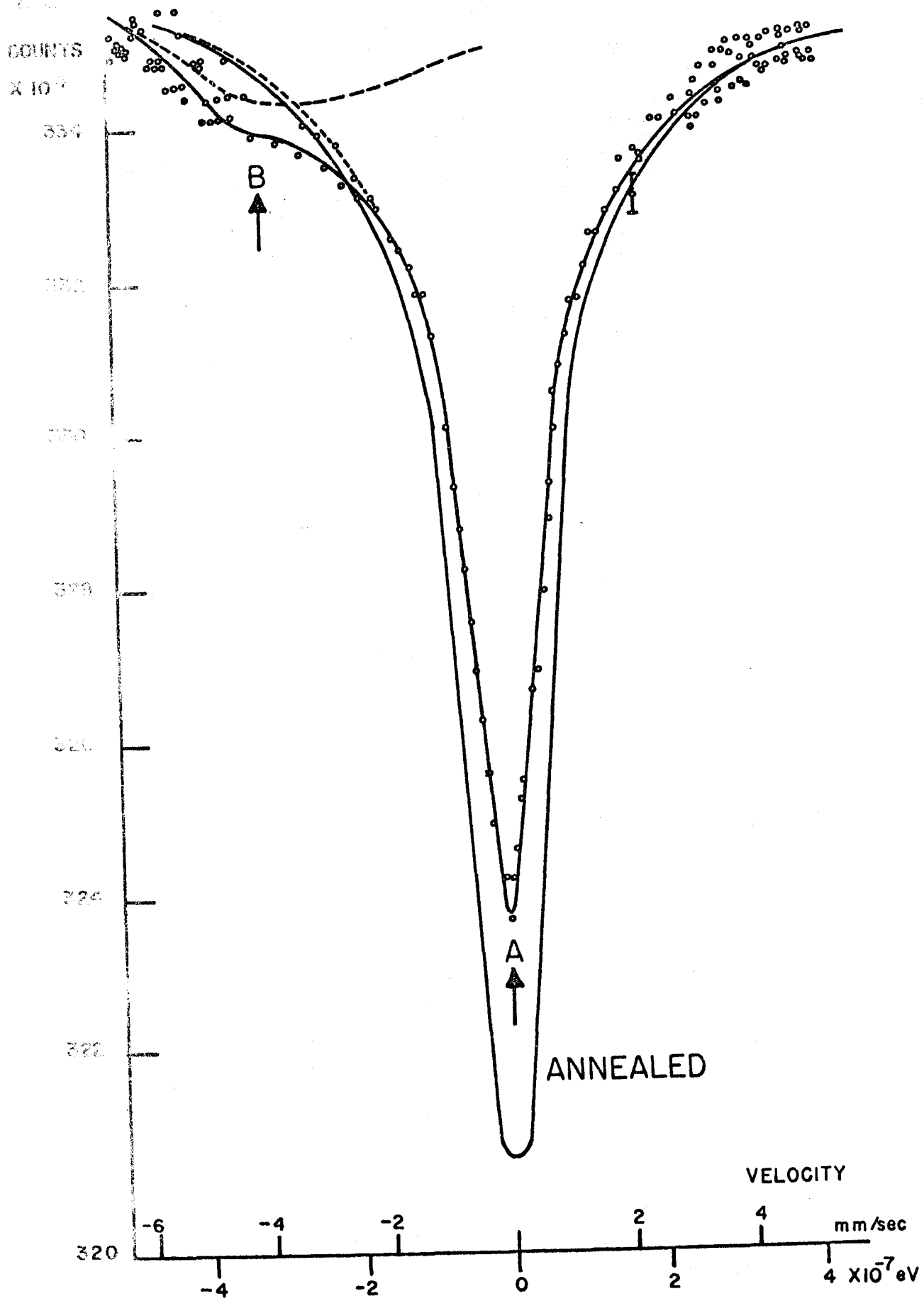

FIG. 3

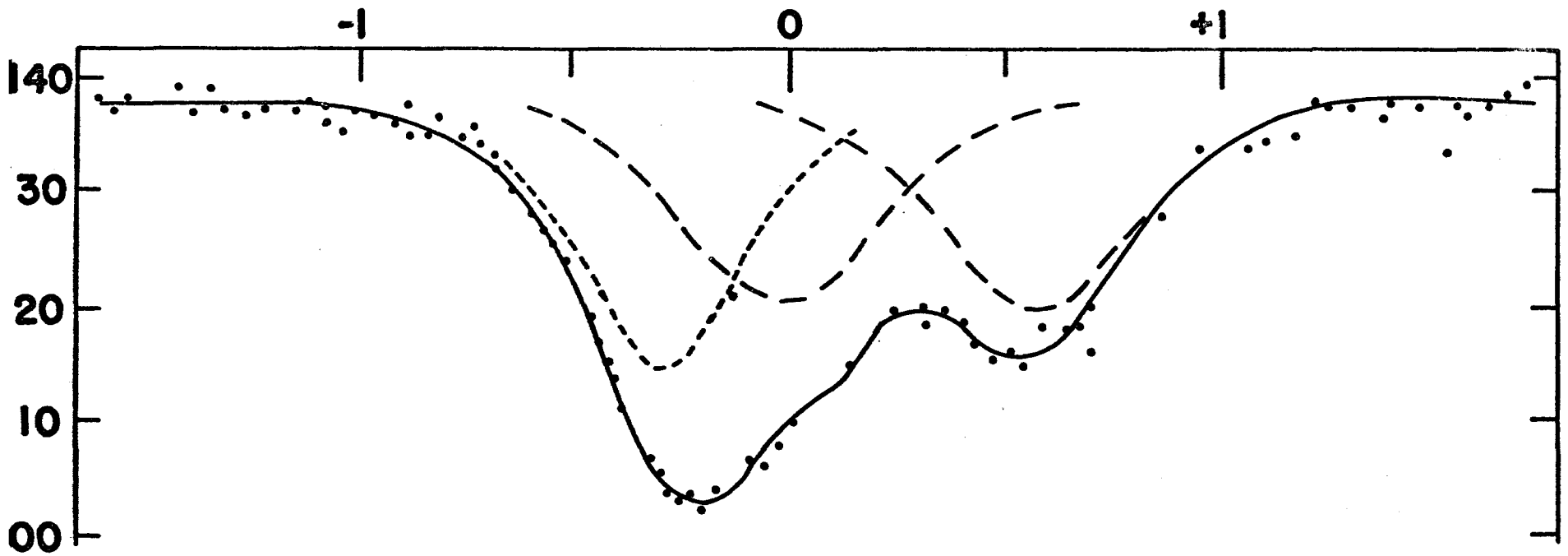
-1
0
+1
140
30
20
10
00

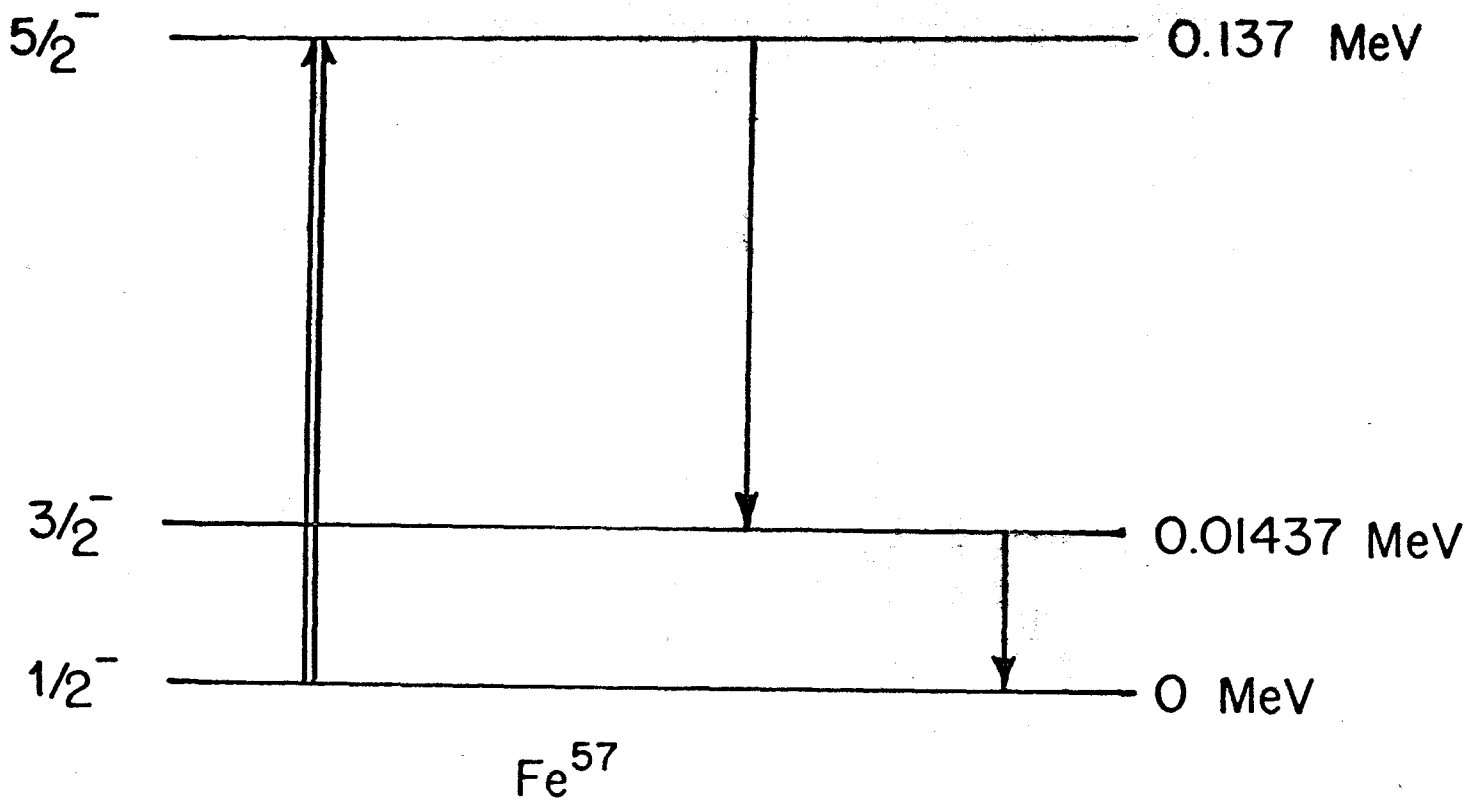

FIG. 10

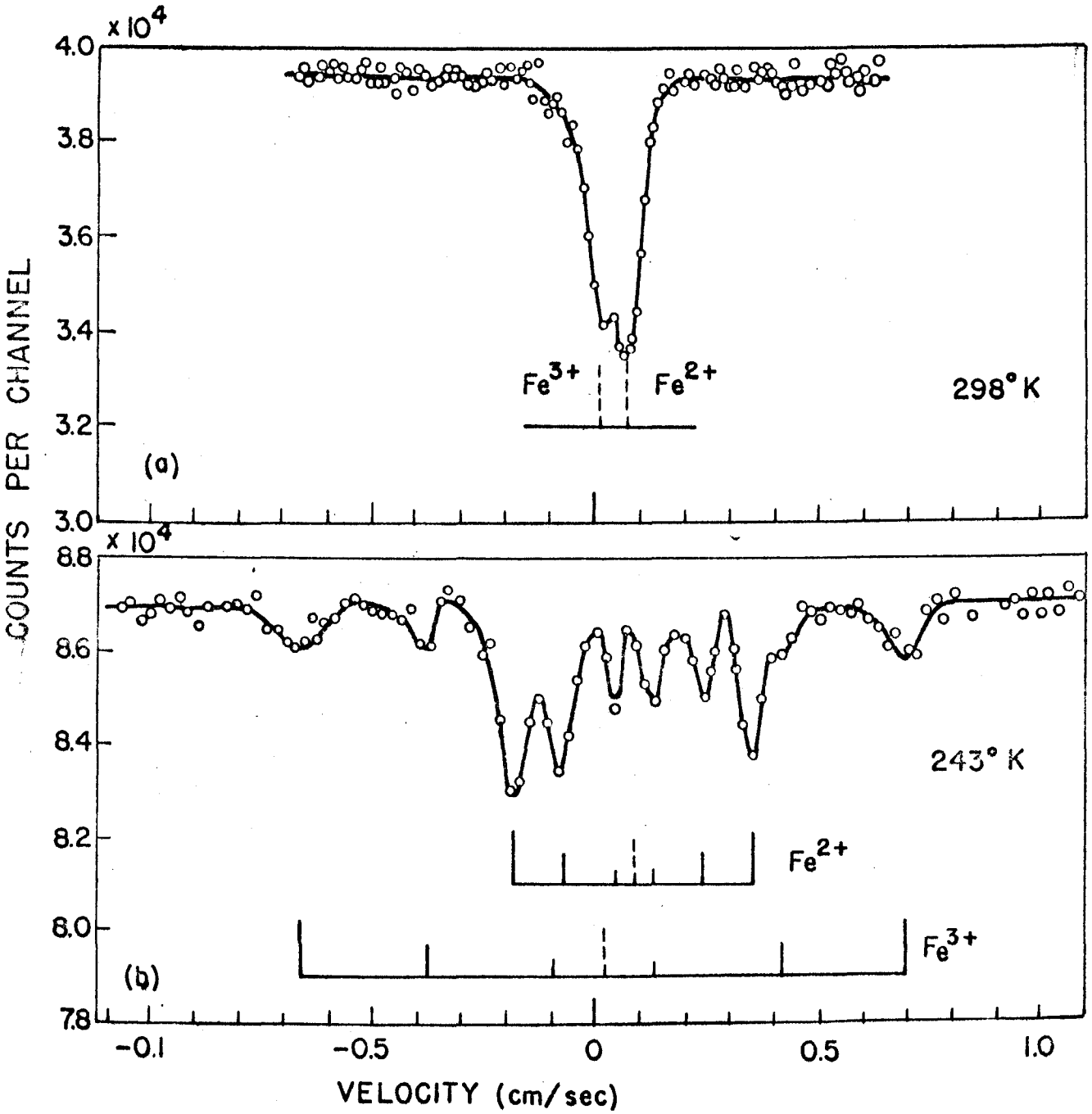
x 10^4
4.0
3.8
3.6
3.4
3.2
3.0
Fe3+
Fe2+
298° K
(a)
COUNTS PER CHANNEL
x 10^4
8.8
8.6
8.4
8.2
8.0
7.8
243° K
Fe2+
Fe3+
(b)
-0.1
-0.5
0
0.5
1.0
VELOCITY (cm/sec)

FIG. 11

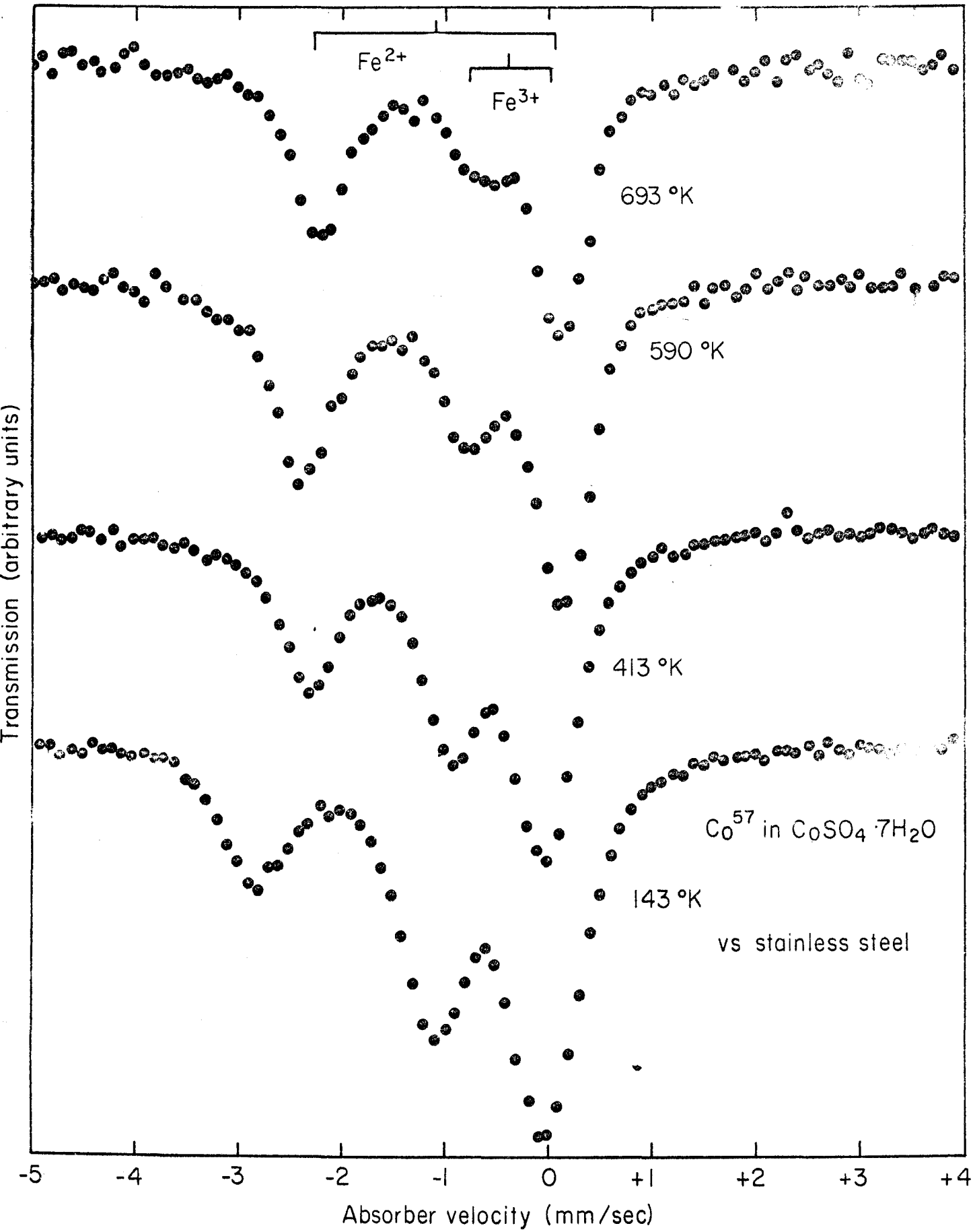
Fe2+
Fe3+
693 °K
590 °K
413 °K
143 °K
Co57 in CoSO4 ·7H2O
vs stainless steel
Transmission (arbitrary units)
-5
-4
-3
-2
-1
0
+1
+2
+3
+4
Absorber velocity (mm/sec)

FIG. 12

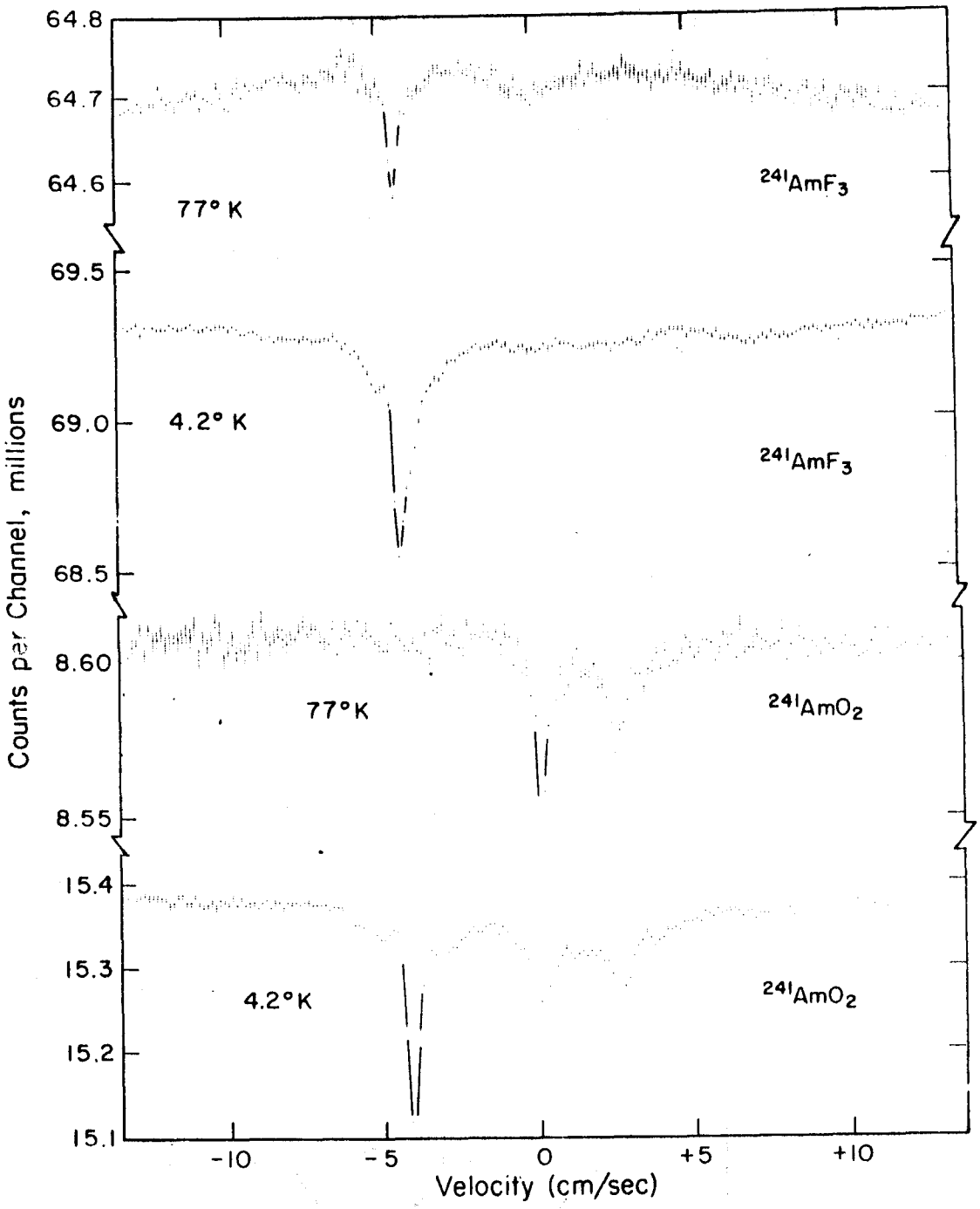

FIG. 11 VELOCITY SPECTRA OF SEVERAL ^{241}Am SOURCES (INSULATORS) SHOWING CHARGE STATES AFTER ALPHA DECAY (NpO_2 ABSORBER).

FIG. 13

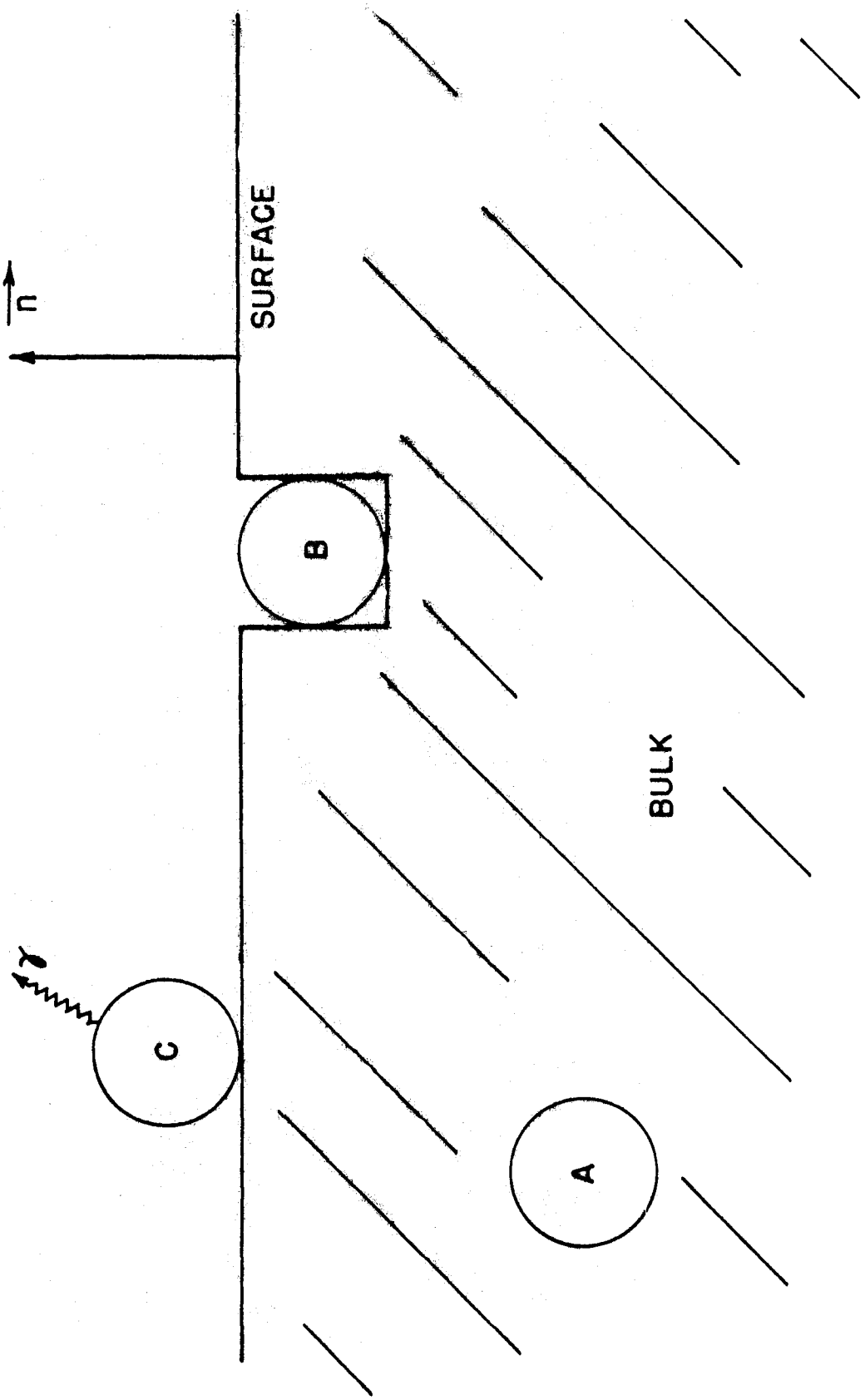

FIG. 14

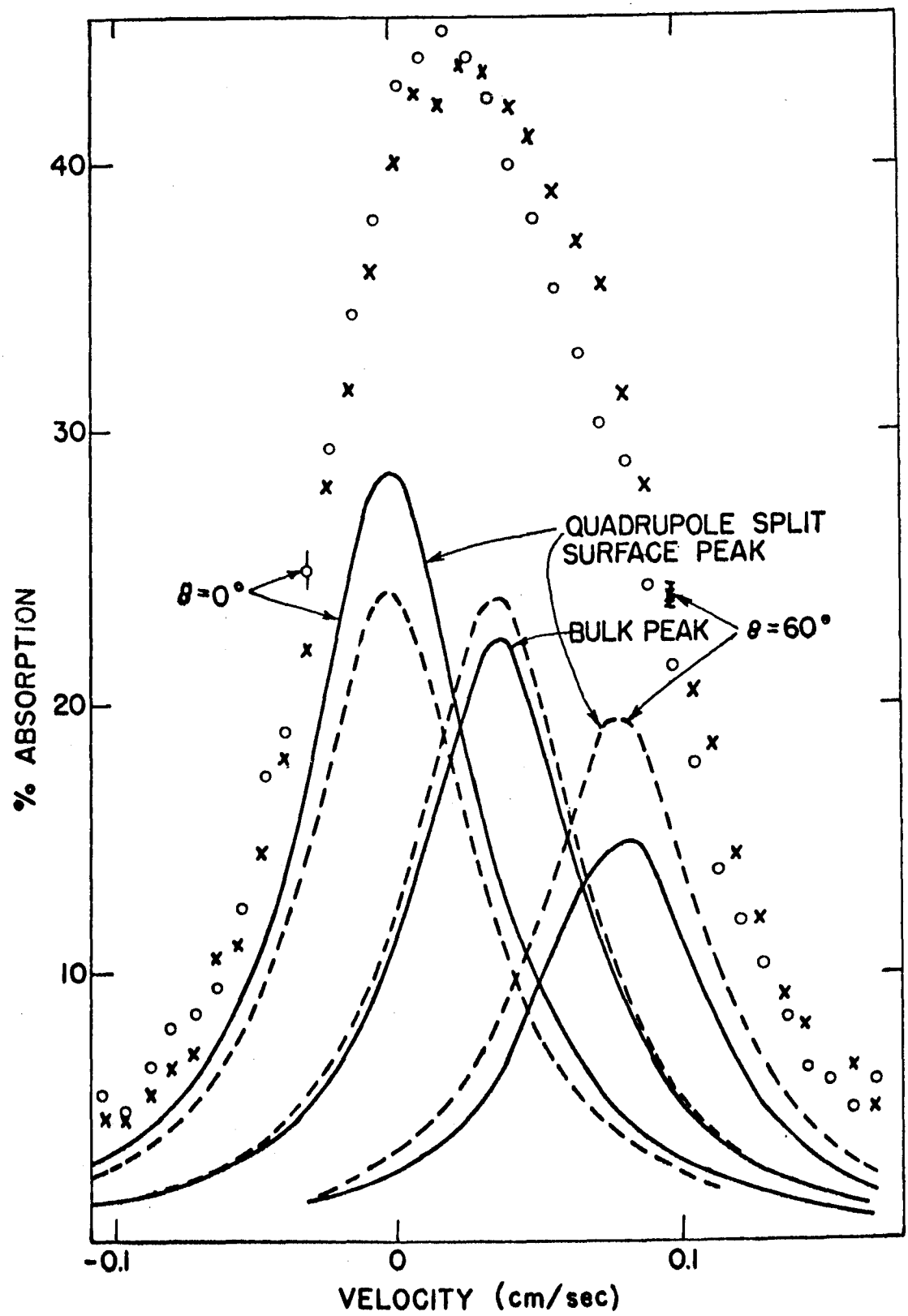
40
30
20
10
% ABSORPTION
QUADRUPOLE SPLIT
SURFACE PEAK
θ=0°
BULK PEAK
θ=60°
-0.1
0
0.1
VELOCITY (cm/sec)

FIG. 15

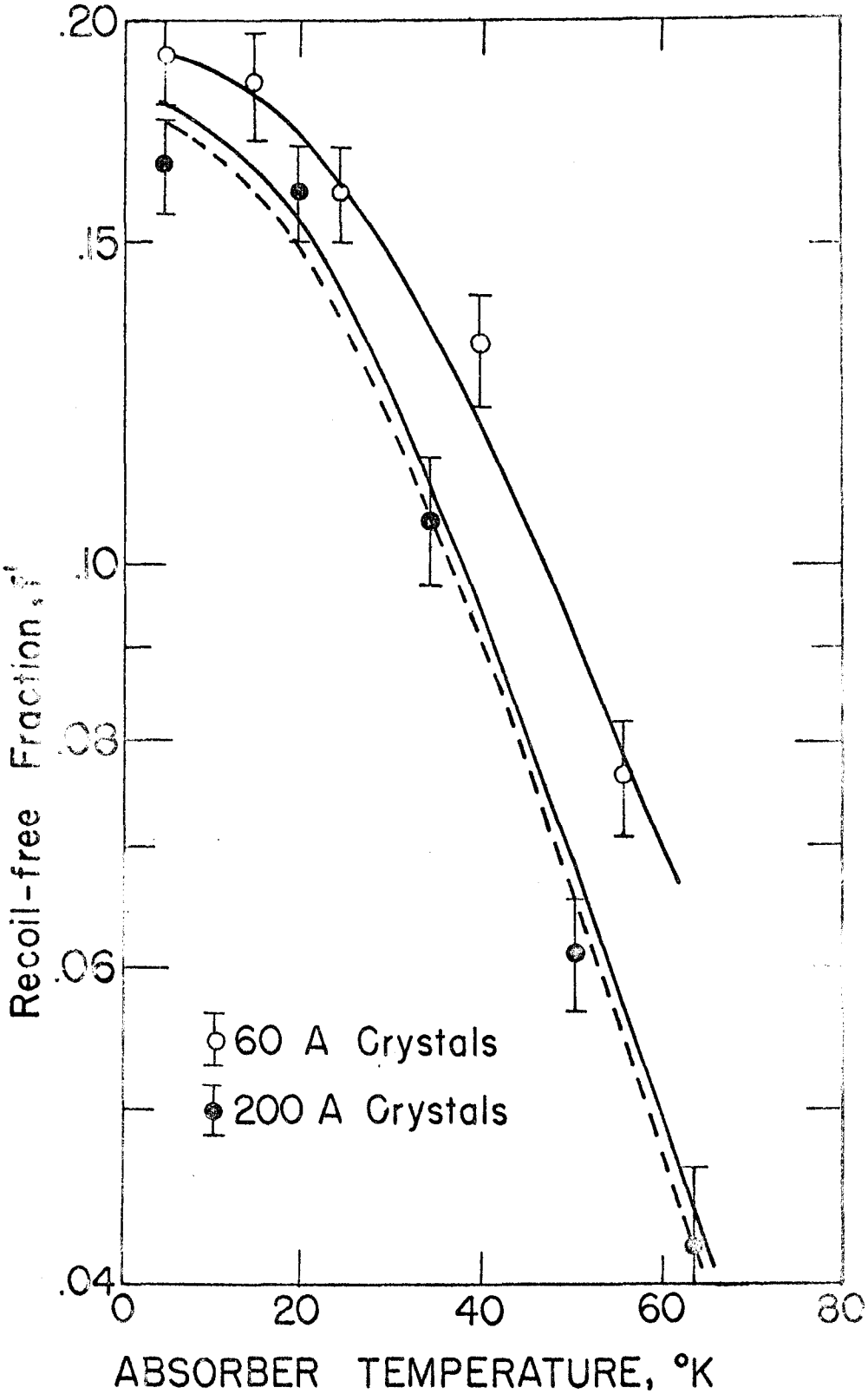
.20
.15
.10
.08
.06
.04
Recoil-free Fraction, f'
60 A Crystals
200 A Crystals
0
20
40
60
80
ABSORBER TEMPERATURE, °K

FIG. 16

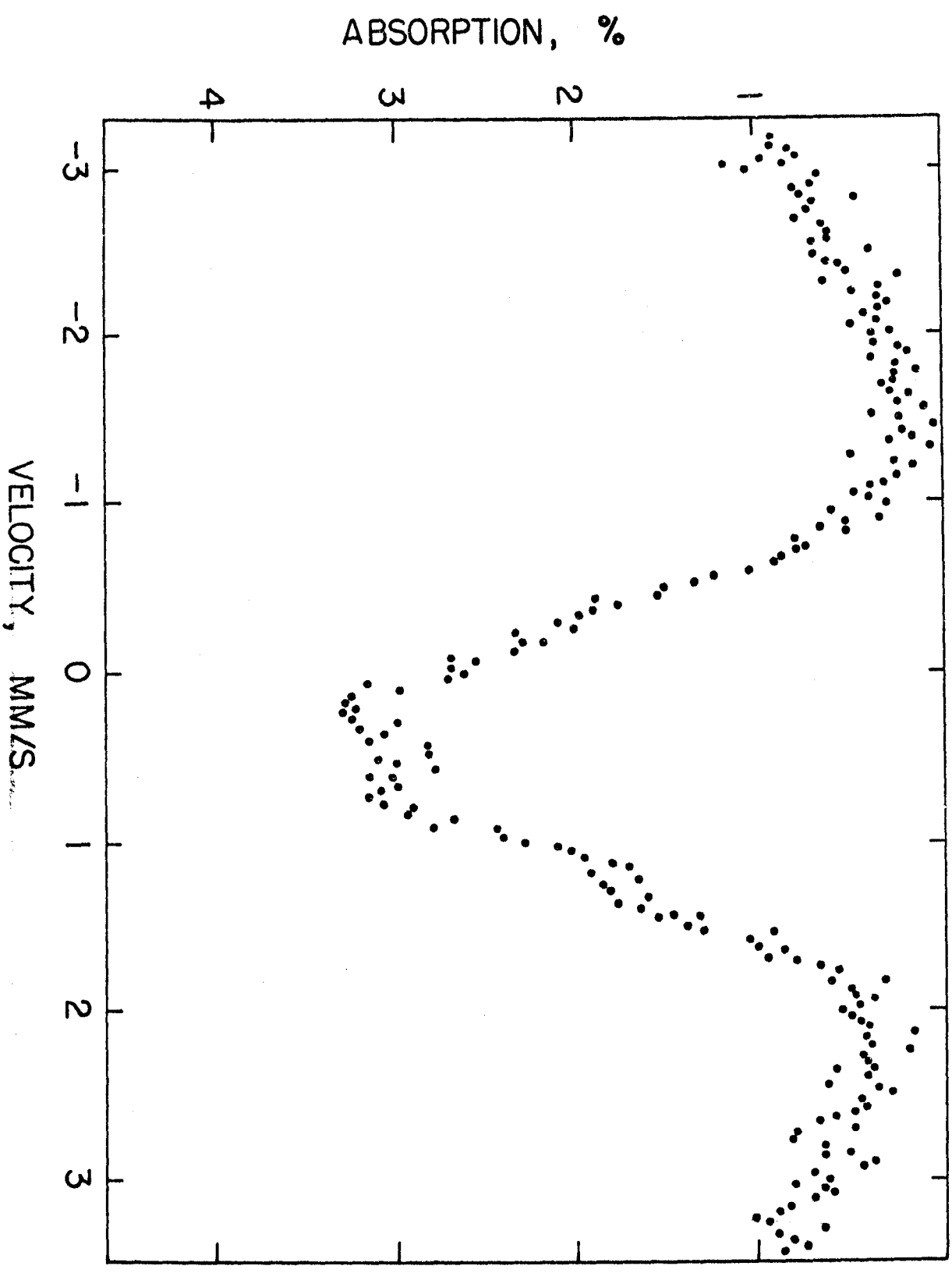

FIG. 17

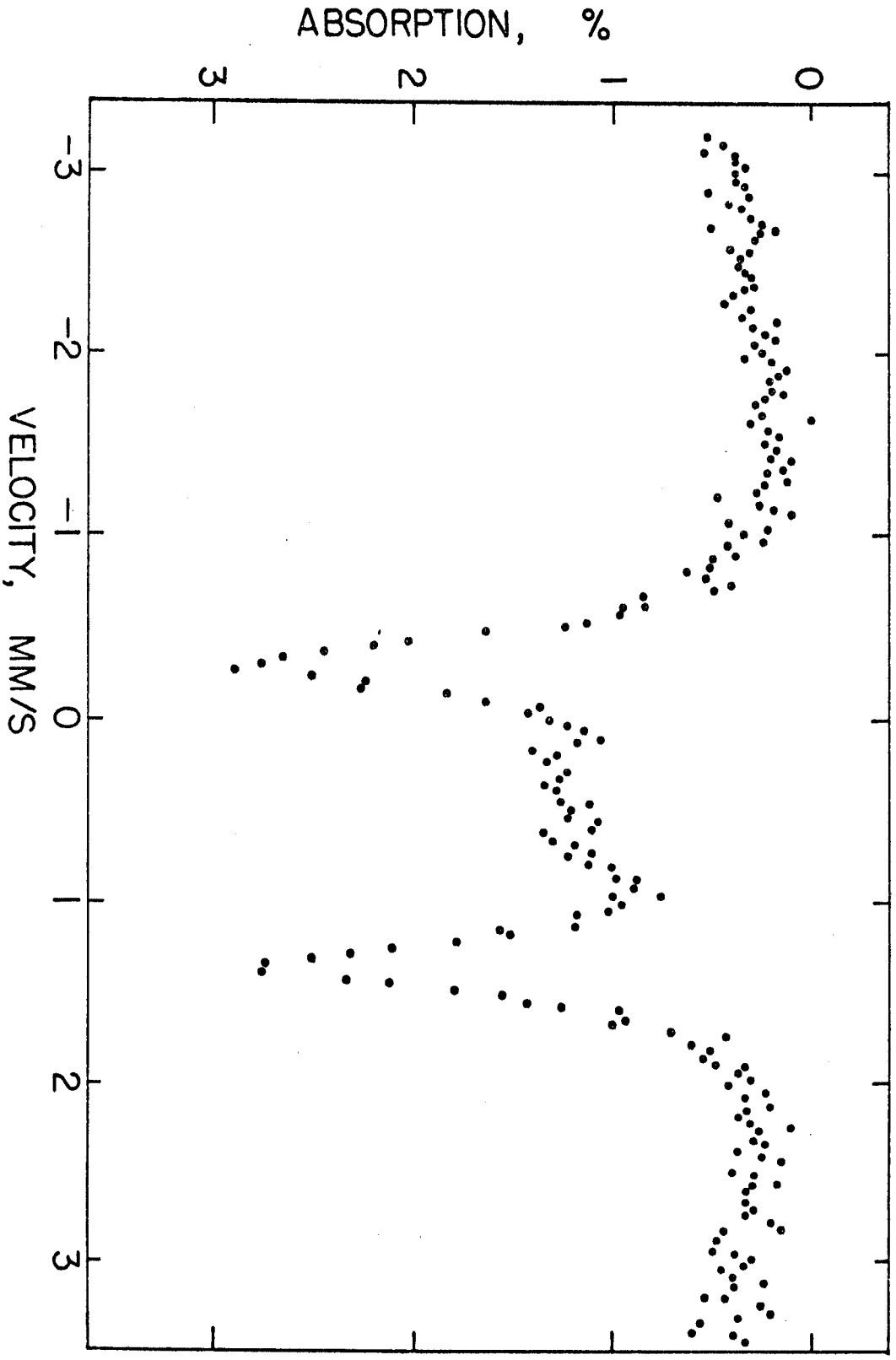

FIG. 18

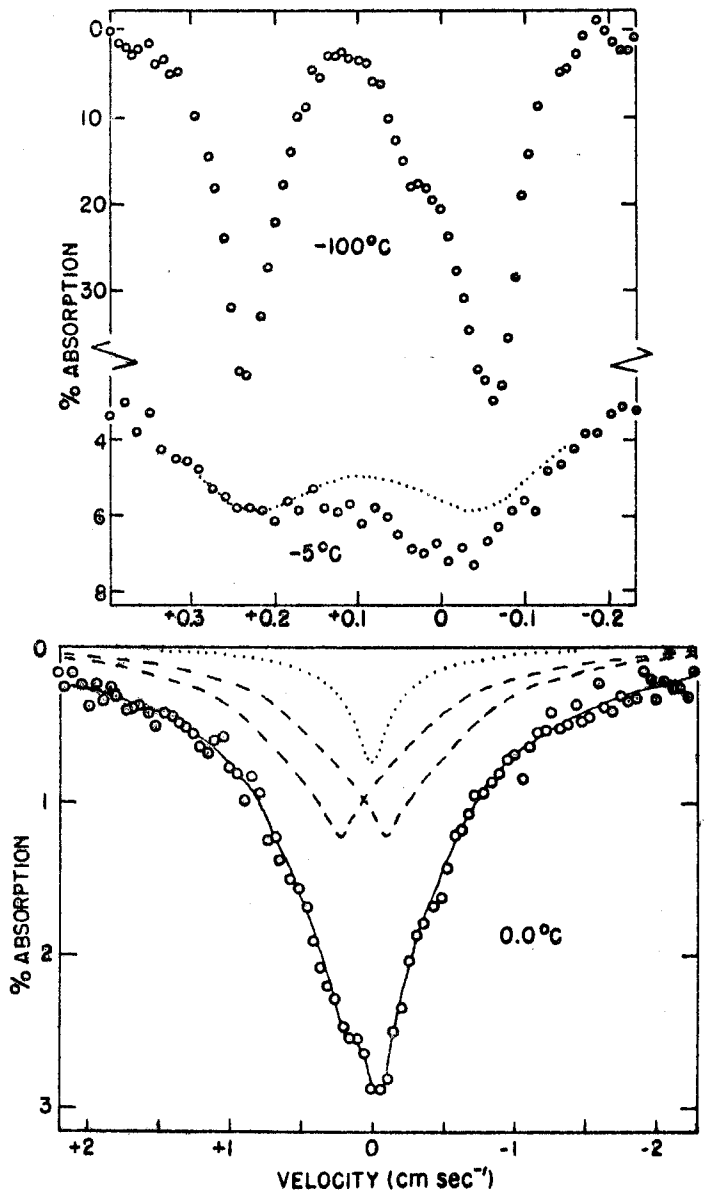
% ABSORPTION
-100°C
-5°C
+0.3
+0.2
+0.1
0
-0.1
-0.2
% ABSORPTION
0.0°C
+2
+1
0
-1
-2
VELOCITY (cm sec⁻¹)

FIG. 19

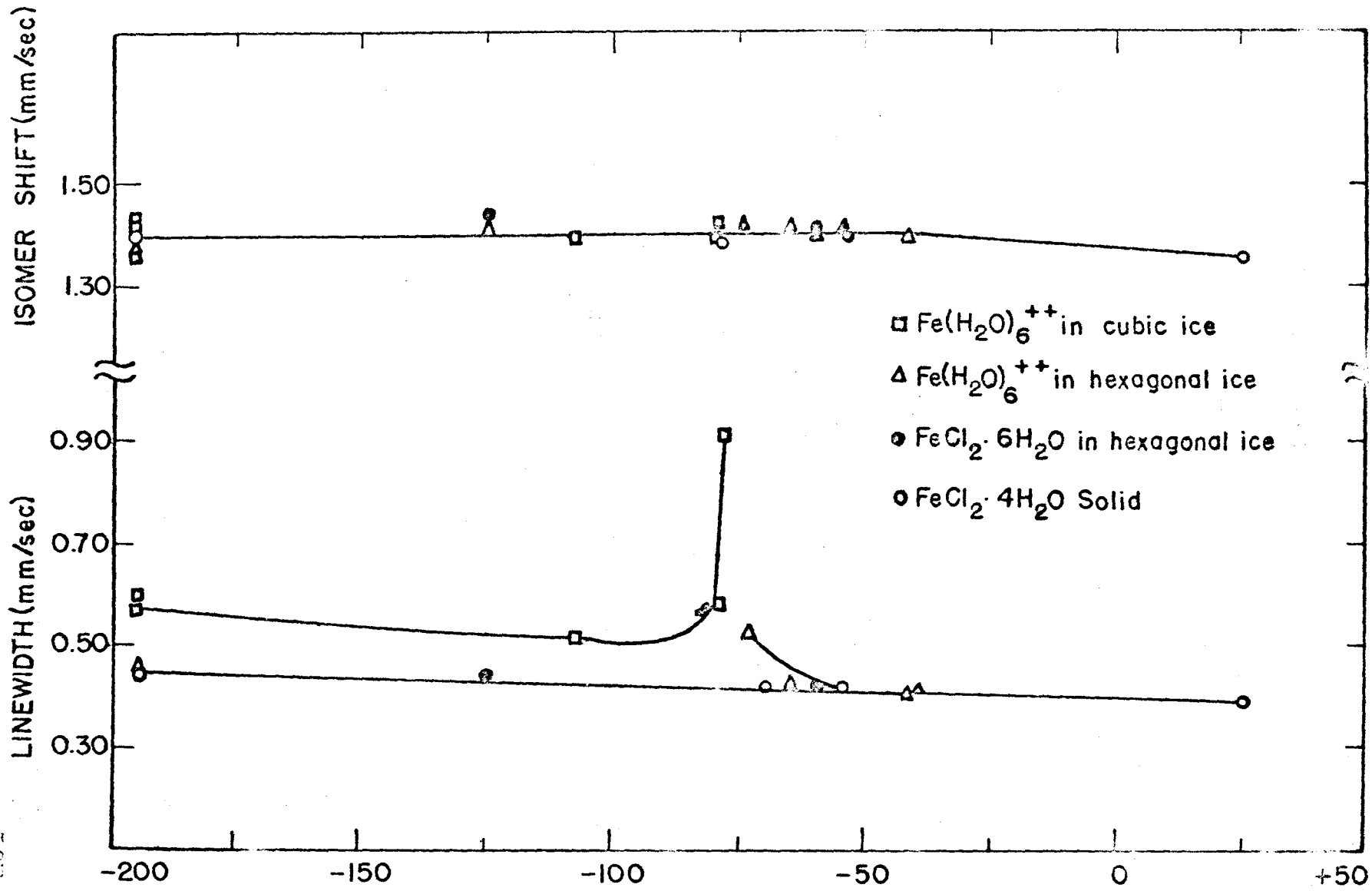
ISOMER SHIFT (mm/sec)
1.50
1.30
LINEWIDTH (mm/sec)
0.90
0.70
0.50
0.30
-200
-150
-100
-50
0
+50
□ Fe(H2O)6++ in cubic ice
△ Fe(H2O)6++ in hexagonal ice
● FeCl2· 6H2O in hexagonal ice
○ FeCl2· 4H2O Solid

FIG. 20

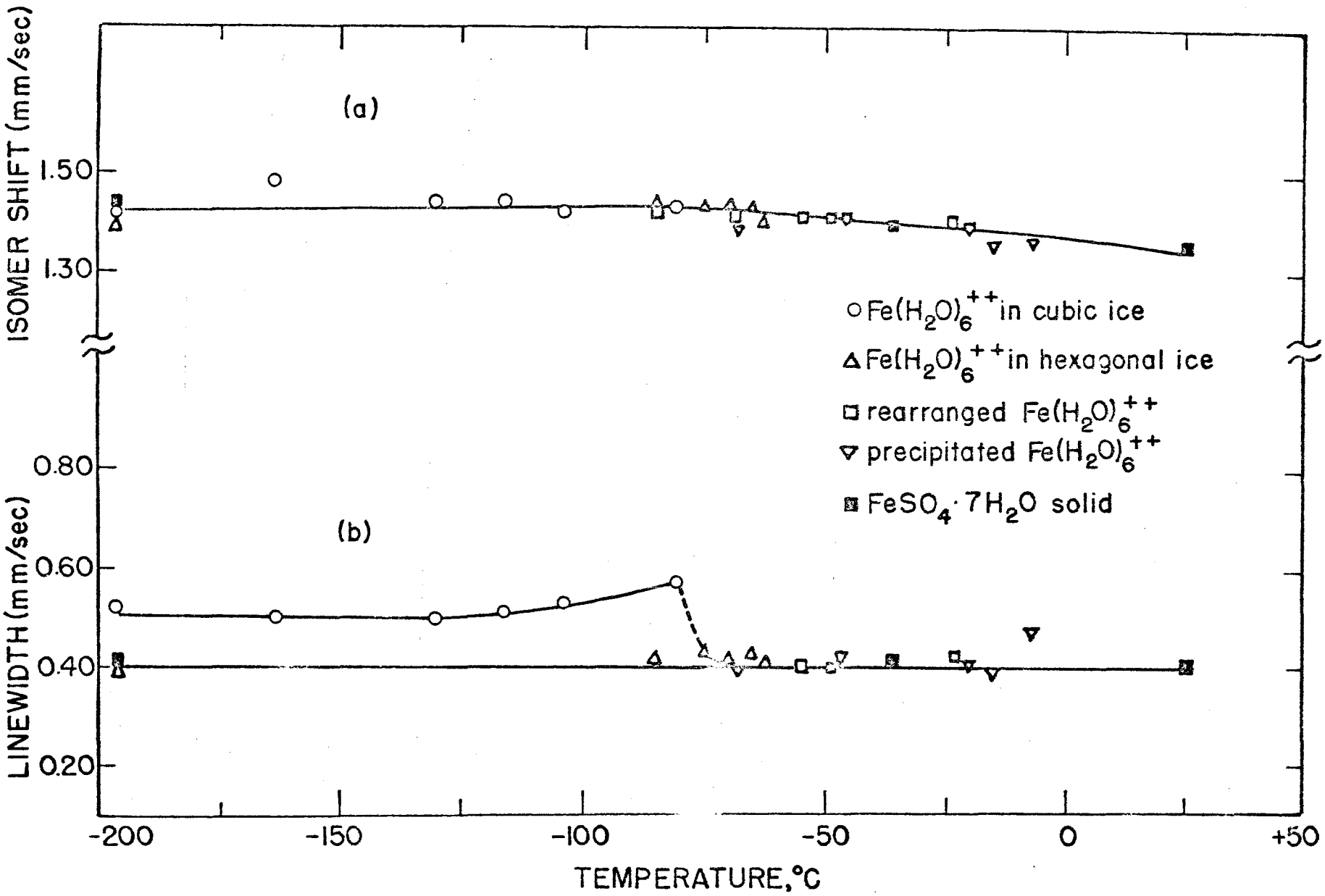
(a)
(b)
ISOMER SHIFT (mm/sec)
LINEWIDTH (mm/sec)
1.50
1.30
0.80
0.60
0.40
0.20
-200
-150
-100
-50
0
+50
TEMPERATURE, °C
○ $Fe(H_2O)_6^{++}$ in cubic ice
△ $Fe(H_2O)_6^{++}$ in hexagonal ice
□ rearranged $Fe(H_2O)_6^{++}$
▽ precipitated $Fe(H_2O)_6^{++}$
■ $FeSO_4 \cdot 7H_2O$ solid

FIG. 21